Available online at www.sciencedirect.com
ScienceDirect
Tectonophysics 425 (2006) 137–157
TECTONOPHYSICS
www.elsevier.com/locate/tecto

The structure, isostasy and gravity field of the Levant continental margin and the southeast Mediterranean area

Amit Segev [a,*], Michael Rybakov [b], Vladimir Lyakhovsky [a], Avraham Hofstetter [b], Gidon Tibor [c], Vladimir Goldshmidt [b], Zvi Ben Avraham [d]

[a] *Geological Survey of Israel, 30 Malkhe Israel Street, Jerusalem 95501, Israel*
[b] *Geophysical Institute of Israel, P.O. Box 182, Lod 71100, Israel*
[c] *Israel Oceanographic and Limnological Research, Israel*
[d] *Department of Geophysics and Planetary Sciences, Tel Aviv University, Ramat Aviv 69978, Israel*

Received 2 January 2006; received in revised form 2 July 2006; accepted 20 July 2006
Available online 14 September 2006

Abstract

A 3-D layered structure of the Levant and the southeastern Mediterranean lithospheric plates was constructed using interpretations of seismic measurements and borehole data. Structural maps of three principal interfaces, elevation, top basement and the Moho, were constructed for the area studied. This area includes the African, Sinai and Arabian plates, the Herodotus and the Levant marine basins and the Nile sedimentary cone. In addition, an isopach map of the Pliocene sediments, as well as the contemporaneous amount of denuded rock units, was prepared to enable setting up the structural map of the base Pliocene sediment. Variable density distributions are suggested for the sedimentary succession in accord with its composition and compaction. The spatial density distribution in the crystalline crust was calculated by weighting the thicknesses of the lower mafic and the upper felsic crustal layers, with densities of 2.9 g/cm^3 and 2.77 g/cm^3, respectively. Results of the local (Airy) isostatic modeling with compensation on the Moho interface show significant deviations from the local isostasy and require variable density distribution in the upper mantle. Moving the compensation level to the base of the lithosphere (~100 km depth) and adopting density variations in the mantle lithosphere yielded isostatic compensation (±200 m) over most of the area studied. The spatial pattern obtained of a density distribution with a range of ±0.05 g/cm^3 is supported by a regional heat flux. Simulations of the flexure (Vening Meinesz) isostasy related to the Pliocene to Recent sedimentary loading and unloading revealed concentric oscillatory negative and positive anomalies mostly related to the Nile sedimentary cone. Such anomalies may explain the rapid subsidence in the Levant Basin and the arching in central Israel, northern Sinai and Egypt during Pliocene–Recent times. Comparison between the observed (Bouguer) gravity and the calculated gravity for the constructed 3-D lithospheric structure, which has variable density distributions, provided a good match and an independent constraint for the large-scale structure suggested and confirmed an oceanic nature for the Levant Basin lithosphere.

Keywords: Middle East; Mediterranean; Levant; Nile cone; Isostasy; Gravity; 3-D model

1. Introduction

We studied the deep lithosphere structure of the southeastern Mediterranean Sea, Sinai plate and the

* Corresponding author. Fax: +972 2 5380688.
E-mail addresses: amit.segev@gsi.gov.il (A. Segev), rybakov@gii.co.il (M. Rybakov), vladi@gsi.gov.il (V. Lyakhovsky), rami@gii.co.il (A. Hofstetter), tiborg@ocean.org.il (G. Tibor), zvi@terra.tau.ac.il (Z. Ben Avraham).

0040-1951/$ - see front matter © 2006 Elsevier B.V. All rights reserved.
doi:10.1016/j.tecto.2006.07.010

northeastern part of the Arabian plate, which comprises the Levant area (Fig. 1). The main structural units of the Levant area are the continental parts of the African, Sinai and Arabian plates separated by major fracture systems (the Dead Sea transform — DST, and the Suez rift), the Levant and Herodotus marine basins, the Cyprus convergent zone (Cyprus Arc) and the continental margins. The area studied, ~540,000 km^2, spreads from the western Herodotus basin through the Nile sedimentary cone and continental margins to the stable part of the Arabian plate on the east and includes the DST plate boundary. In order to minimize the interruption from the near active plate boundaries, the Cyprus convergent zone (Cyprus Arc) on the NW, and the Red Sea spreading center on the SE are not included in the area studied. The Eratosthenes Seamount, which is commonly interpreted to be a small continental fragment (Makris et al., 1983; Makris and Wang, 1994; Ben Avraham et al., 2002), separates between the Levant and the Herodotus marine basins.

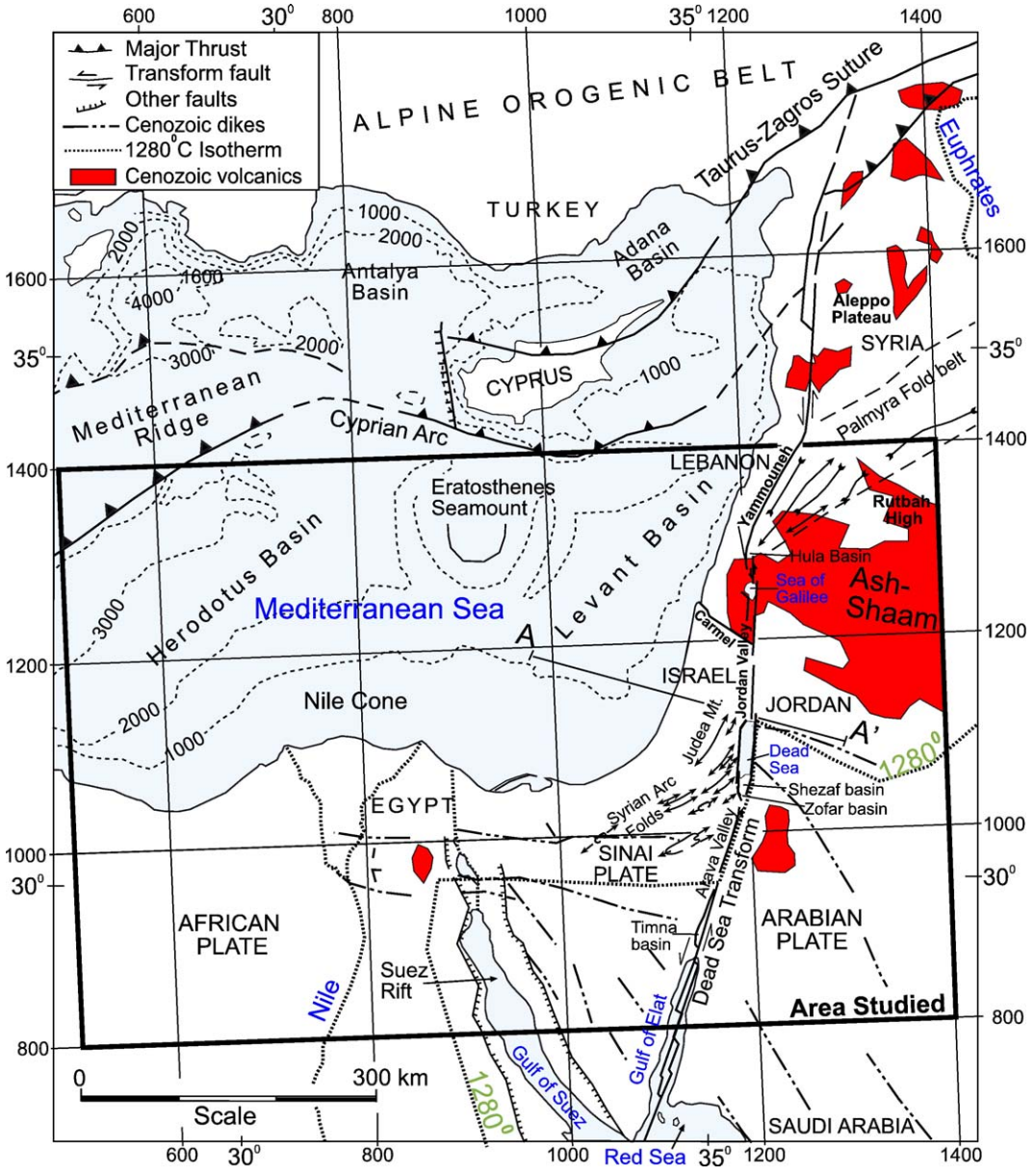

Fig. 1. Major tectonic elements and distribution of Cenozoic volcanic fields of the eastern Mediterranean area; location of the study area (black frame). The thick dotted line represents the 1280 °C isotherm in the lithospheric mantle is according to Camp and Roobol (1992).

The principle goals of this study were:

(1) to establish a detailed 3-D layered structure of the Levant lithosphere plates, including densities of each layer. These layers were constructed using up-to-date published geophysical and geological data including topography, bathymetry, seismic refraction and reflection, gravity, magnetism, deep boreholes and surface geology.
(2) to identify compensated and non compensated regions affected by recent sedimentary loading and active tectonics by local isostatic compensation modeling. Furthermore, this modeling provides the constraint for the compensation level (Moho or the base of the mantle lithosphere) and density distribution in the mantle lithosphere.
(3) to study the influence of the Pliocene to Recent sedimentary loads of the Nile sedimentary cone as well as that within the DST and the Suez tectonic basins on the vertical isostatic motions by regional flexure modeling.
(4) to provide independent verification for the suggested lithosphere structure and additional constraints for active tectonic regions (obtained from the isostasy modeling), local density heterogeneities and database artifacts by using gravity modeling.

2. Geologic and tectonic setting

The composition and internal structure of the study plates are the consequence of the complex geological history since late Precambrian times that can be divided into six major tectono-magmatic events (Segev et al., 1999; Segev, 2000): (1) the Precambrian Pan-African orogenic phase (ended ~600 Ma); (2) the late Precambrian to Early Cambrian (ended ~530 Ma) post-orogenic extensional phase associated with voluminous alkaline magmatism; (3) the Middle Cambrian to Permian stable platform phase; (4) the Permian to Late Cretaceous Tethyan plume activities, which created the Levant westward-thinning, passive continental margins and the Palmyra tectonic belt; (5) the Late Cretaceous to Eocene convergent phase; (6) the Oligocene to Recent Afar plume activity, which formed the present-day structure and morphology.

The Dead Sea transform, the main active plate boundary between the Arabian and African-Sinai plates (Fig. 1), accumulated a differential movement of ~100 km (Freund et al., 1970; Garfunkel, 1981). Sneh (1996) suggested that most of the left-lateral displacement took place between the late Early Oligocene to early Middle Miocene (ca. 30–16 Ma, biostratigraphical age). During the Oligocene and Miocene times both sides of the DST were part of a continuous low-relief landscape, which drained to the Mediterranean (e.g., Picard, 1951; Garfunkel and Horowitz, 1966; Garfunkel, 1981; Zilberman, 1992; Matmon et al., 2003). Matmon et al. (2003) assume that uplift and denudation rates were equal and the low relief landscape was retained. The major change in the morphology, or the establishment of the DST drainage system and the deposition of clastic sediments within the narrow "rift valley" morphology occurred in the Early Pliocene (5.2±0.1–3.5±0.1 Ma, Ar/Ar ages from Heimann et al., 1996) (Picard, 1951; Bentor and Vroman, 1960; Sneh, 1999). The asymmetrical topography and structure across the DST have been studied since more than a century ago (Lartet, 1869; Picard, 1966). The shallow part of the cross section presented in Fig. 2 is based on the compilation of the Levant crustal structure by Garfunkel (1998). The depth to the Moho boundary is after Hofstetter et al. (2000), and the constraint for the depth to the lithosphere–asthenosphere boundary is discussed below. Wdowinski and Zilberman (1997) studied the large-scale structure across the DST and show that the rift's eastern margin is regionally uplifted toward its axis, whereas the rift's western margin is downflexed toward its axis and defines a wide asymmetrical monocline (Fig. 2B). ten Brink et al. (1990) followed by Hofstetter et al. (2000) used geophysical evidence for their quantitative model of the crust across the same profile north of the Dead Sea. Although this profile crosses the DST, in part where the topography is almost symmetrical, the westward thinning of the crust is the prominent feature. Local thinning of the crust east of the Dead Sea is an important modification of Hofstetter et al. (2000) (Fig. 2). DESERT Group (2004) indicates asymmetric topography of the Moho under the DST and suggests that it was caused by the left-lateral motion along it.

The Suez rift, about 70 km wide and 500 km long, forms the northwestern branch of the Red Sea. It partially separates the Sinai block from the African continent (Fig. 1) and is considered to be the tectonic boundary between the African and the Sinai plates (McKenzie et al., 1970). The rift tectonics is well documented (e.g., Garfunkel and Bartov, 1977; Courtillot et al., 1987; Evans, 1988; Patton et al., 1994; Steckler et al., 1998), although the total amount of its opening and the timing of movements are still debated. The extension and rifting in the Gulf of Suez took place mainly during the Miocene (e.g., Patton et al., 1994; Steckler et al., 1998). By the Middle Miocene (Eyal et al., 1981; Feinstein et al., 1996) or even earlier, in the late Oligocene

(Sneh, 1996), the DST developed and replaced the Suez rifting as the active plate boundary north of the Red Sea. Therefore the post Middle Miocene evolution of the Gulf of Suez was typified by continuing uplift of the rift flank and subsidence of the rift center (Steckler et al., 1998).

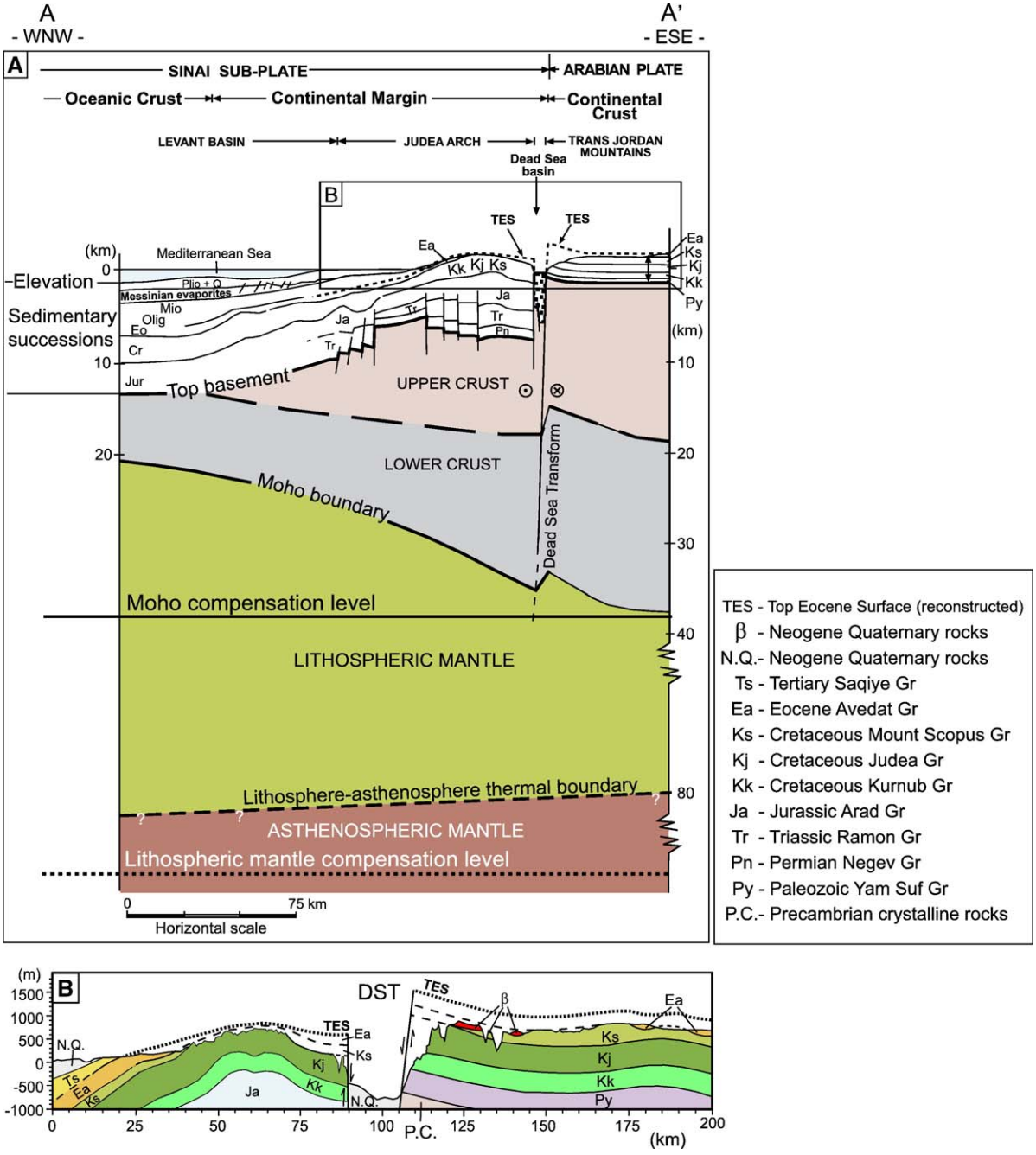

Fig. 2. (A) Schematic cross section through the Levant lithosphere showing the interfaces and the layers of the present study. The shallow part is modified after the review of Garfunkel (1998); and the Moho is modified after Hofstetter et al. (2000) (see text for further discussion). The frame represents the location of the detailed cross section (B). Jur: Jurassic sediments; Cr: Cretaceous sediments; Eo: Eocene sediments; Olig: Oligocene sediments; Mio: Miocene sediments; Plio+Q: Pliocene to Quaternary sediments. (B) Representative geological cross section across the DST shows the large-scale structure and the major rock units. Note the reconstructed top Eocene (TES) marker (after Wdowinski and Zilberman, 1997).

The Levant continental margin formed during the evolution of the Neo- and the Meso-Tethys (or southern Neo-Tethys) oceans, estimated to have transpired in the Late Triassic–Early Jurassic (Garfunkel, 1998, Segev, 2002). Whether the Levant Basin is built of oceanic crust (e.g., Makris et al., 1983; Makris and Wang, 1994; Ben Avraham et al., 2002) or of continental crust (e.g., Woodside, 1977; Hirsch et al., 1995) is still a debate in the scientific community.

The Tethys Ocean's final regression over the continental parts of the Levant took place at the end of the Eocene when a westward to northwestward regional drainage system formed (e.g., Picard, 1951; Garfunkel and Horowitz, 1966; Zilberman, 1992; Garfunkel and Ben Avraham, 1996; Begin and Zilberman, 1997; Avni, 1998). Oligocene uplifts and denudations truncated mostly parts of the Eocene carbonate units, predominantly exposing the preexisting Late Cretaceous Syrian Arc fold belt. The Miocene times are typified by tectonic and magmatic activities (Giannérini et al., 1988; Shaliv, 1991; Segev, 2000; Ilani et al., 2001). This activity, as well as the later volcanism, crosses the DST without preferential magmatism along this plate boundary and without significant thermal activity, as indicated also by the 37.6 mW m^{-2} averaged measured heat flow in the Dead Sea (Ben Avraham et al., 1978).

The principal vertical movements that produced the present-day morphology started in the Pliocene (Picard, 1951; Bentor and Vroman, 1960; Matmon et al., 2003) after widespread volcanism in the Ash-Shaam and other volcanic fields on the Arabian plate (Giannérini et al., 1988; Heimann et al., 1996; Ilani et al., 2001). These vertical movements have been associated with normal faulting followed by broad structural arching (40–60 km wide) between the Mediterranean and the DST (Fig. 2B) (Salamon, 1987; ten Brink et al., 1990; Matmon et al., 2003). The amplitude of this arch is 200–300 m in the Galilee (Matmon et al., 2003), ~400 m in central Israel, Judea Mountains (Wdowinski and Zilberman, 1997) and ~200 m in the Negev (Salamon, 1987). The Nile delta and cone, which

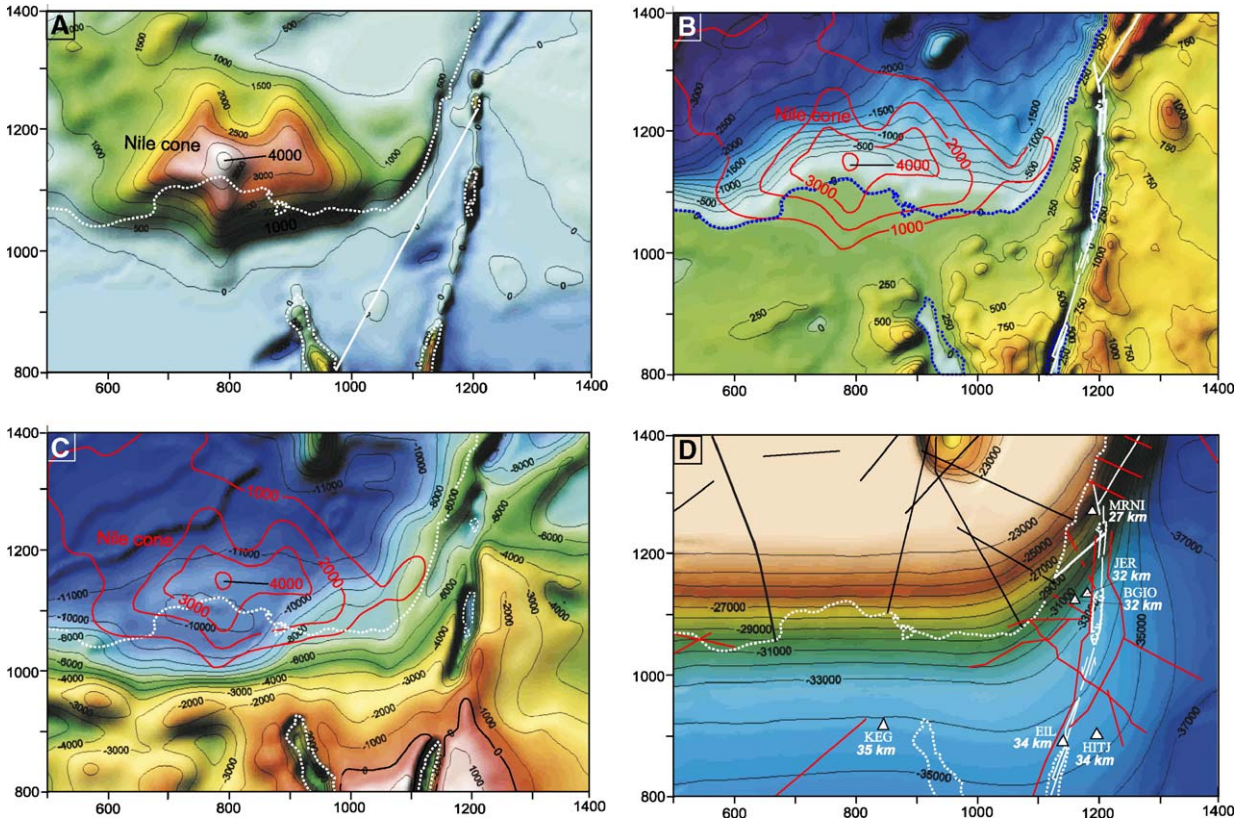

Fig. 3. (A) Thicknesses (m) of sedimentary layers denudated from the continental regions (negative values) and accumulated within the marine and continental basins since the Pliocene. Here and in the following maps the coastlines (black or white) are marked for orientation. (B) The measured elevation, topography and bathymetry of the area studied (in meters). Here and in the following maps the DST major faults and isopach contours of the Nile cone are marked for orientation. Sources: HYDRO1K 1 km grid and 1.0′ Grid of HDNO (for details see text). (C) Structural map of the top basement (in meters; after Rybakov and Segev, 2004). (D) Structural map of the Moho boundary (in meters) according to the data of inferred depth to the Moho interface achieved by seismic methods (for sources see text). Note the different structure of the continental margin in the northeastern part of the Mediterranean Sea, the Lebanese region, and in the southern part, the Egyptian region.

was initiated in the early Pliocene (Ross and Uchupi, 1977; Said, 1981), comprise up to 4000 m of clastic sediments that cover a significant part of the southern Levant basin (Fig. 3A). This Pliocene–Recent sedimentary mass, or the Nile cone, which is the principal load on the Sinai plate, generally overlies the Messinian evaporites, but the salt layers are particularly thin or absent beneath the thick part of the Nile cone and thicken outward as a result of gravity-driven tectonics of the viscous salt layers (Abdel Aal et al., 2000; Loncke et al., 2002; Gaullier et al., 2002). Similarly, large volumes of clastics have been transported from the Nile delta and deposited along the continental margin of Israel. Basin analysis of the Late Tertiary Levant continental margin (Tibor et al., 1992) reveals that the tectonic

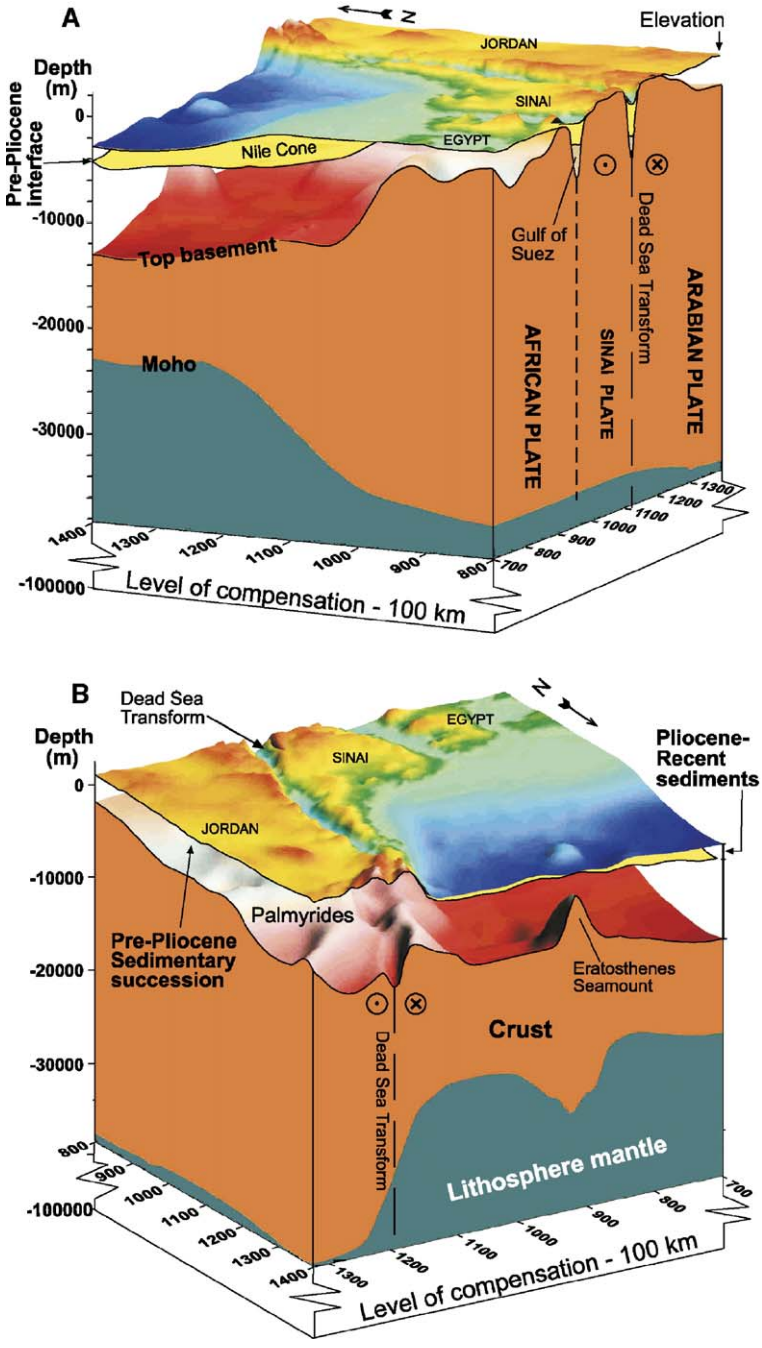

Fig. 4. The constructed 3-D structure of the Levant lithosphere exhibiting its four layers. (A) View from the southwest, (B) view from the northeast.

subsidence there follows the expected thermal subsidence for mature passive margins, whereas during the Pliocene an increase in tectonic subsidence (the Pliocene "anomaly") occurred in the Israel shelf area and coastal plain. This Pliocene "anomaly", which ranges from about 450 m in the south to 250 m in the north, was interpreted as a result of a regional process, such as the flexural response of the lithosphere to the uplift of the Judea Mountains or to the sedimentary load of the Nile cone (Tibor et al., 1992).

3. The 3-d Structure and the density variations of the Levant lithosphere

Fig. 4 demonstrates the regional 3-D model structure of the Levant area constructed using four layers bounded by five interfaces (see Fig. 2 for cross section). The layered structure includes the sedimentary Pliocene–Recent and Cambrian to Pliocene succession separated into two sedimentary layers, crystalline crust and mantle lithosphere. The interfaces were mapped through collection, integration and interpolation of up-to-date data from various sources. The present study first adopted the available low-resolution database of the team of the Institute for the Study of the Continents in Cornell University, and later modified it by better resolution and updated data. The current work compiled geological and geophysical, i.e., gravity, seismic profiles and teleseismic observations to build the structure of the lithospheric plates on both sides of the DST. A brief discussion of the data sets used for constructing these interfaces and constraints for the density of each layer are presented in this section.

3.1. Sedimentary succession

The entire sedimentary succession is delimited at the top by the elevation (topography and bathymetry), and at the base, by the top of the crystalline basement interface. Splitting the whole sedimentary succession into two layers enables simulating the effect of the Pliocene–Recent Nile sedimentary cone on the vertical motions. The 3-D model (Fig. 4) shows only the accumulated part of Pliocene–Recent sediments corresponding to the positive values of the layer thickness, while the negative values stand for the eroded parts (Fig. 3A) (Table 1). Both positive and negative values are converted to sedimentary loading or unloading for the regional isostatic calculations presented in the following section.

3.1.1. The elevation interface

The topographic dataset for the area studied on land is the HYDRO1K 1 km grid produced by the U.S. Geological Survey (Fig. 3B). The bathymetric database for the Mediterranean area is from the available 1.0′ Grid of HDNO (Head Department of Navigation and Oceanography — USSR Ministry of Defense, St. Petersburg).

3.1.2. Pre-Pliocene reconstructed interface

This structural map was calculated by reducing the Pliocene–Recent isopach map (loading), mainly in the southeastern Mediterranean region, and supplementing the contemporaneous amount of denuded rock units (unloading) from the Arabian, Sinai and African continental parts (Fig. 3A). The Oligocene–Miocene deep erosion and sedimentation were not included in the present study. The dataset for the Pliocene–Recent isopach map includes several minor tectonic basins along the DST that accommodate such sedimentary fill. Most of the dataset is related to the thickness of the Pliocene–Recent sequences in the southeastern Mediterranean (Levant) basin. The top Messinian evaporate (Hsu et al., 1977) reflector in this basin defines the base of the Pliocene sequences there. This reflector is well defined by a single and by multi-channel seismic profiles, and several two-way travel time (TWT) maps were produced by a number of marine seismic studies (e.g., Limonov et al., 1992; Burollet and Gennesseaux, 1998; Gennesseaux et al., 1998). The conversion of the TWT to thickness is controversial and, therefore, several different interpretations have been suggested. Tibor et al. (1993) stated that the maximum thickness at the peak of the Nile delta cone is ~3500 m, whereas Abdel Aal et al. (2000) reported ~4000 m. We calculated the thickness of the Nile deposits since the Pliocene in two stages: first, construction of a TWT map to the top Messinian reflector; and then, conversion of the TWT to the sediment thickness. The TWT map to this reflector is

Table 1
Thickness of the Pliocene–Recent sediments within tectonic basins

Basin	Thickness (km) since Miocene/Pliocene	Sources
Gulf of Elat	~6/–	Ben Avraham (1985)
Timna	1.4/0.5	Segev et al. (1999)
Zofar	–/0.2	Frieslander (2000)
Shezaf	~3.7/–	Frieslander (2000)
Dead Sea	~12 at the center,	Zak (1967); Frieslander (2000)
	6 at the north/~6	Ginzburg and Ben Avraham (2001)
Sea of Galilee	~8/2.4	Marcus and Slager (1985); Ben Avraham et al. (1996); Ginzburg and Ben Avraham (2001)
Hula basin	–/2.4	Heimann (1990)
Gulf of Suez	–/~2 at the south, ~1 at the north	Garfunkel and Bartov (1977)

based on several sources from Lebanon, Israel and Sinai (Ginzburg et al., 1975; Ryan and Cita, 1978; Ben Avraham and Mart, 1981; Mart and Eisin, 1982), sources from Egypt (Lort et al., 1974; Woodside, 1977; Mascle et al., 2000; Bellaiche et al., 2002), sources from southeastern Cyprus (Ben Avraham et al., 1995), and from regional-scale data (Ross and Uchupi, 1977; Limonov et al., 1992). The conversion of the TWT to sediment thickness is based on the average velocity within the Pliocene–Recent sediments calculated from well logs and multichannel seismic profiles (e.g., Lort, 1973; Ross and Uchupi, 1977; Limonov et al., 1992; Tibor et al., 1992; Brian, 1998; Rybakov et al., 1999; Badri et al., 2000; Loncke et al., 2002). To simplify the conversion, the sedimentary column is divided into three layers with average velocities 2 km/s, 2.5 km/s and 2.8 km/s for TWT below 2 s, between 2 and 3 s, and above 3 s, respectively.

The internal basins along the DST vary in dimensions and presumably had different modes of formation. In our study we considered only the thickness of the Pliocene–Recent sediments within these basins as follows (Table 1):

Relatively thick and extensive areas of basalt were added to the sedimentary layer (Fig. 5A): (1) the Miocene rift-related Lower Basalt Formation, mainly in the subsurface, delineated according to Shaliv (1991), up to 650 m; (2) the Pliocene–Recent flood basalts of the northwestern part of the Harrat Ash Shaam exposed volcanic field, averaging about 200 m thick. The Miocene basalts were considered in our calculations as denser lithology at the top of the pre-Pliocene

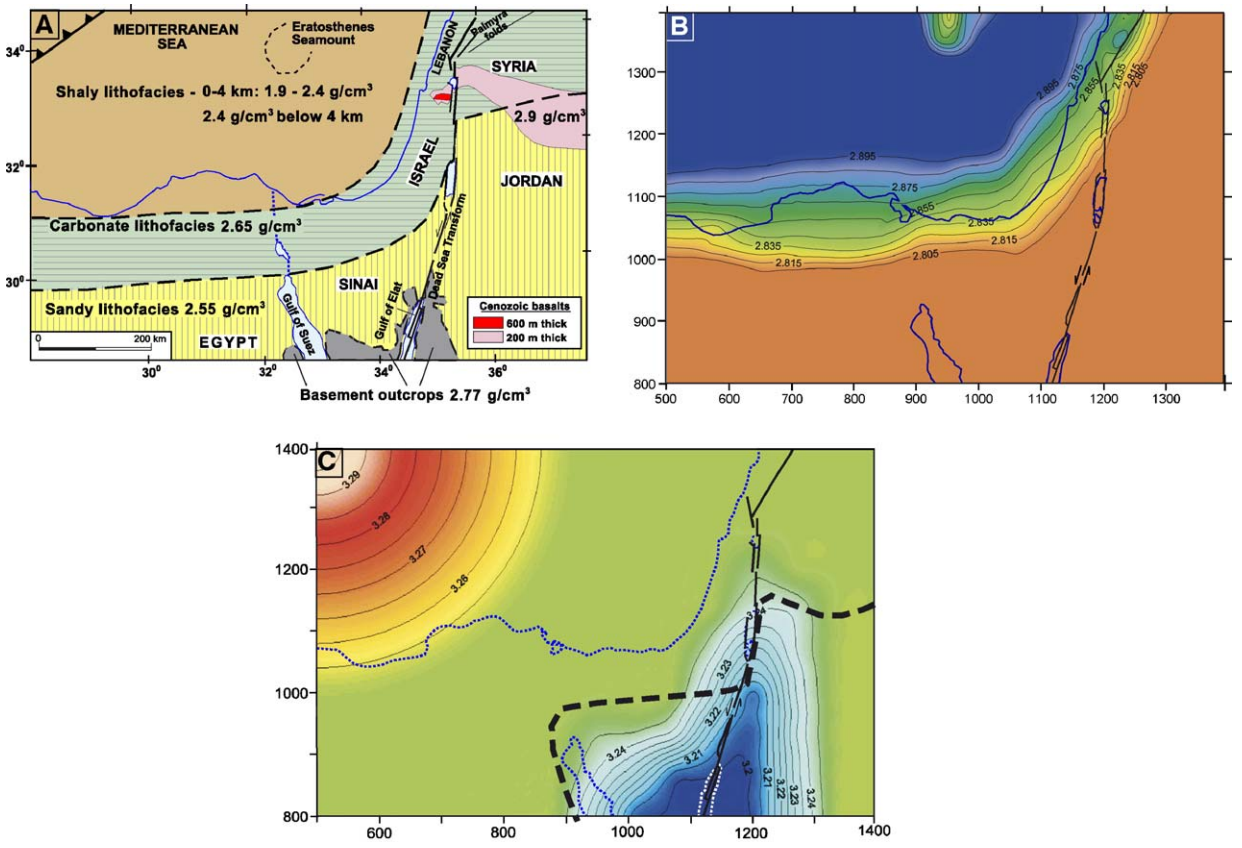

Fig. 5. (A) Distribution of lithofacies and Cenozoic basalts. Note the average density values for each sedimentary lithofacies. (B) Density distribution in the crystalline crust calculated by weighting the thickness of the mafic crust having a density of 2.9 g/cm^3, with the thickness of the felsic crust having a density of 2.77 g/cm^3. (C) Density distribution within the lithospheric mantle. The average density value of 3.25 g/cm^3 is decreased (down to 3.20 g/cm^3) in the region north of the Red Sea spreading center, corresponding to the higher temperature. This density variation compensates the positive isostatic anomaly of region 1 on Fig. 6A, which fits well with the outline of the potential temperatures in the lithospheric mantle according to Camp and Roobol (1992) (Fig. 1). Contrarily, the density was increased (up to 3.30 g/cm^3) in the colder region of the old oceanic crust in the Herodotus basin. This density variation compensates the negative anomaly in region 2 on Fig. 6A.

sedimentary column, whereas the Pliocene basalts were calculated as part of the load.

The amount of Pliocene–Recent denudation on the continental part of the study area was obtained using geological considerations, mainly the estimated thickness of the Miocene sequence that eroded since the Pliocene. For our large-scale study we generalized the eroded thickness of the Pliocene sediments as noted by several researchers (Zilberman, 1992; Avni, 1998 and personal communication, 2004; Calvo, 2002 and personal communication, 2004; A. Sneh, personal communication, 2004). The amount of denudation is digitized and combined with the isopach data given in Fig. 3A.

3.1.3. Density variations of Pliocene–Recent sediments

ten Brink et al. (1990) and Hofstetter et al. (1991, 2000) suggested an average density of 2.15 g/cm^3 for the Pliocene–Recent sediments (predominantly the Nile delta cone) in the SE Mediterranean Sea. However, borehole log data (Rybakov et al., 1999) demonstrate significant depth-dependence of the sediment density from 1.86 g/cm^3 at shallow depths to 2.4 g/cm^3 at ~2.4 km depth. Hence, we evaluated quantitatively the downward (to 2.4 km depth) increase in density within the Mediterranean basins, depending on compaction processes, by using the concept of Rybakov et al. (1999) based on borehole log data. These authors suggested a third-order polynomial equation that enables a best-fit approximation for the density-versus-depth curve:

$$\rho = 1.86 + 0.165D - 0.02267D^2 + 0.0012D^3$$

where ρ is density (g/cm^3) and D is depth (km). Using their equation, the average density (ρ_a) of a layer with thickness H is:

$$\rho_a = \frac{1}{H}\int_o^H \rho(D)\mathrm{d}D = 1.86 + 0.0825H - 0.00756H^2 + 0.003H^3$$

This relation was used for the top sediments throughout the entire Mediterranean area down to ~2.4 km. Below this depth the compacted fine clastic rocks (marls, shales and turbidities) reach their maximal average density of 2.4 g/cm^3.

3.1.4. The top of the crystalline basement interface

A low-resolution data set of this interface, underlying the sedimentary succession, was compiled based on seismic data published by Seber et al. (1997) (Fig. 3C). Recently, Rybakov and Segev (2004) presented the most updated map of the top basement, which significantly improved the resolution of the previous dataset for Jordan, Israel, Sinai and the Levant Basin. Their compilation is based on the latest results from deep boreholes, seismic refraction profiles, and quantitative interpretation of magnetic anomalies. They summarized in detail their sources and methods, and their dataset is used in the present study, including the consequent isopach map of the sedimentary succession between the top basement and the base Pliocene sediments (Fig. 4). The available geophysical data does not support the existence of any depression beneath the Nile cone; on the contrary, it even sustains a small basement high (e.g., Sahagian, 1993). This leads to a close anti-correlation between the isopach contours of the Nile cone and those of the entire sedimentary succession that could be explained by several reasons, among them: enhanced compaction of the underlying strata due to load of the Nile cone sediments; post-Messinian erosion by the paleo Nile River at the time of the Mediterranean regression; lateral flow of the thick Messinian evaporate succession as a result of the Nile cone loading; and others.

3.1.5. Density variations of Cambrian to Pliocene sediments

Based on lithostratigraphic evidence, the area studied was divided into three generalized zones or lithofacies belts (Fig. 5A), excluding the surroundings of the Red Sea, Gulf of Suez, and the Gulf of Elat (Aqaba), where Precambrian crystalline basement rocks are exposed. The lithofacies belts are: (a) sandy; (b) carbonate; and (c) shaly. This subdivision was carried out according to the predominant lithology in each of the lithofacies zones. The average density values were adopted from a petrophysical study of Rybakov et al. (1999). The contacts between these lithofacies are gradational and match the relief of the top crystalline basement (Fig. 3C). The sandy lithofacies (Fig. 5A), which covers the southern and southeastern parts of the area and has an average density of 2.55 g/cm^3, typifies the shallow platform part of the Arabian–Nubian (African) Shield during Phanerozoic times (Druckman et al., 1975; Klitzsch, 1991; Al-Husseini, 1997; Hirsch et al., 1998). The belt-like carbonate lithofacies, with an average density of 2.65 g/cm^3, follows the Mesozoic to Recent continental margins of Egypt (Klitzsch, 1991) and Israel, continuing toward the ENE and overlapping the Triassic (Druckman et al., 1975) up to Late Cretaceous shallow continental margins. The shaly lithofacies overlaps the deep marine basins of the previous Tethys Ocean and the present Mediterranean Sea. The variable densities of the upper part (0–4 km) are described above, and that of the compacted lower part (below 4 km) is 2.4 g/cm^3. In addition, regions covered by significant

basaltic fields and thick tectonic basins along the DST and within the Gulf of Suez were also digitized. The density of the basalt is 2.9 g/cm^3 and the variable density of the young basin fill was calculated in the same way as the above-mentioned young sediments.

3.2. The crystalline crust

The crystalline crust is delimited at the top by the top of the basement interface discussed above (Fig. 3C) and at the base by the interface of the Moho discontinuity.

3.2.1. The Moho discontinuity

Construction of the dataset for the Moho boundary is based on long-term deep seismic investigations in the Middle East starting with a seismic study of the DST and the continental margin by Ginzburg et al. (1979) (Fig. 3D). Makris et al. (1983) presented results of a deep seismic refraction study in the Levant basin. Seismic refraction data from Jordan were reported by El-Isa et al. (1987); these results have been summarized in the geographic information system (GIS) by Seber et al. (1997). Recently, Ben Avraham et al. (2002) presented deep refraction profiles from across the Eratosthenes Seamount, Levant basin. Improvement for the constructed Moho (Fig. 3D) came from deep refraction profiling (DESERT Group, 2004), teleseismic tomography (Hofstetter et al., 2000) and analysis of receiver function (Hofstetter and Bock, 2004). The location of the broadband stations MRNI, JER, BGIO and EIL in Israel, HITJ in Jordan, and KEG in eastern Egypt and the depth to the Moho boundary obtained by these teleseismic observations is depicted in Fig. 3D.

The lower/upper crust transition (Conrad boundary) is used only for vertically averaged density calculations. The seismic data from Jordan and Israel (Ginzburg et al., 1979; El-Isa et al., 1987) led Batayneh and Al Zoubi (2001) to place it beneath Jordan at a depth of ~18 km. Westward this boundary is interpreted to meet up with the top basement interfaces at the very end of the continental margins (Fig. 2).

3.2.2. Density variations of crust

Several geophysical investigations combining seismic profiles with gravity data in different parts of the area have suggested various lateral and depth density distributions in the crust; however, the interface between the upper felsic and lower mafic crust is not well constrained for the Levant area. Makris et al. (1983) and ten Brink et al. (1990) suggested a uniform lower crust with a density of 2.90 g/cm^3. Best et al. (1990) used a slightly lower value of 2.86 g/cm^3 for the lower crust in the Rutba uplift (south of the Palmyrides). Batayneh and Al Zoubi (2001) used 2.86 to 2.91 g/cm^3, and Ben Avraham et al. (2002) used 2.80 g/cm^3. Similarly, the density of the upper crust is also controversial. Best et al. (1990) used 2.73 g/cm^3, whereas Batayneh and Al Zoubi (2001) used densities of 2.76 to 2.78 g/cm^3, ten Brink et al. (1990), 2.70 g/cm^3, and Ben Avraham et al. (2002), 2.75 g/cm^3. Summarizing these studies led us to conclude that the average density of the crystalline crust gradually changes across the continental margin, depending mostly on the thickness of the upper felsic crust, which wedges out seaward. This structural change results in a significant difference in the crustal thickness and causes density disparity. Therefore, the lateral variation of the crustal density (Fig. 5B) was calculated by vertical averaging of the density of the mafic lower crust (2.9 g/cm^3) and those of the felsic upper crust (2.77 g/cm^3) weighted according to their thickness.

3.3. The mantle lithosphere

The mantle lithosphere is delimited at the top by the Moho discontinuity and at the base by the interface of the lithosphere–asthenosphere boundary.

3.3.1. The lithosphere–asthenosphere boundary

The boundary between the mantle lithosphere and the asthenospheric mantle may be defined by two different parameters (e.g., Watts, 2001): (a) the base of a seismic Low Velocity Zone (LVZ), or a seismic boundary; (b) a thermal boundary. For a newly formed surficial oceanic lithosphere that cooled down along ~80 Ma, Parsons and McKenzie (1978) suggested that the seismic boundary of the top rigid part of the lithosphere (top of the thermal boundary layer) is equivalent to the 1100 °C isotherm. However, the thermal boundary is located in the base of the thermal boundary layer, which is equivalent to the 1330 °C isotherm and overlies the viscose mantle. According to these authors after 80 Ma the depth to the seismic boundary is ~80 km and to the thermal boundary, ~100 km. Poudjom Djomani et al. (2001) suggested a thermal boundary ranging between 1250 and 1300 °C, whereas Jimenez-Munt et al. (2003), in their study of the Middle East, located it at the 1350 °C isotherm. Using teleseismic observations at broadband stations (Fig. 3D), Hofstetter and Bock (2004) suggested locating the seismic boundary of the Sinai plate at a depth of 65–70 km (with an error of ± 10%). In keeping with Parsons and McKenzie (1978), such an oceanic lithosphere value is in accord with a thermal boundary at a depth of 90 km. Petrological evidence from Harrat Uwayrid (near the SE corner of the area studied) on the Arabian plate led Henjes-Kunst (1989) to suggest that the thermal boundary there is at a shallow depth of ~60 km. McGuire and Bohannon (1989)

estimated the depth to this boundary beneath Harrat Kishb at ~75 km, and Altherr et al. (1990) came to the same conclusion for all the Arabian harrats. Therefore, a similar depth (~75 km) to this boundary may be indicated for Harrat Ash-Shaam at the eastern part of the area studied. Petrological evidence from the Neogene volcanic rocks in northern Israel led Weinstein (1998) to suggest depths to the thermal boundary shallower than 80–90 km. In a review of the surface heat flow in the Mediterranean area Jimenez-Munt et al. (2003) located the thermal boundary of the continental parts at a depth of ~80 km and deeper (~120 km) at the cold oceanic lithosphere of the Herodotus basin, the NW part of the area studied. The suggested ~80 km depth of the lithosphere–asthenosphere boundary of the continental parts fits well with the above-mentioned seismic and petrologic evidence, and was therefore adopted in our study.

3.3.2. Density variations of mantle lithosphere

The constraint of the density in the lithosphere mantle is limited. Ben Avraham et al. (2002) used a uniform density of 3.25 g/cm^3 for gravimetric models in the eastern Mediterranean. We adopted this value as representing most of the area studied, except for the Gulf of Elat and Gulf of Suez and surroundings, and the Herodotus basin. Camp and Roobol (1992) suggested a northward expansion of heating within the lithospheric mantle of the Arabian plate. Feinstein et al. (1996) compiled the heat flow data for the northern Red Sea area and showed that the heat flow values decrease from hundreds mW/m^2 in the Red Sea spreading center to 57 mW/m^2 at the northern most tip of the Gulf of Suez and 64 mW/m^2 at the northern tip of the Gulf of Elat. The fast decrease of the heat flow from the Red Sea axis toward its margins is also discussed by Steckler et al. (1998). Maurath and Eckstein (1990) reported a regional heat flow density in Israel of 52 mW/m^2. This value was obtained by averaging measurements of 23 deep boreholes. Moreover, they measured an anomalously low heat flow of 36.5 mW/m^2 in the central Dead Sea–Jordan Valley. Furthermore, based on analysis of the local seismicity, Aldersons et al. (2003) suggested that the surface heat flow in the Dead Sea basin is below 40 mW/m^2. They argue that these low values of heat flow are a good indication that the lower crust might be cool and brittle and may explain the deep seismogenic zone under the Dead Sea basin. These results indicate that the temperature of the lithospheric mantle is relatively high along the Gulf of Elat and becomes normal in the vicinity of the Dead Sea basin. Based on this evidence, we locate the low density anomaly of the lithosphere mantle in the southeastern part of the study area (Fig. 5C).

The decrease trend of the surface heat flow from the Levant coastline seaward was reported by Pollack et al. (1993) and later by Jimenez-Munt et al. (2003). Accordingly, a gradual increase of the mantle lithosphere density is suggested in the northwestern part of the study area (Fig. 5C). In the next section we discuss the effect of density variations in the lithospheric mantle, up to $\Delta\rho = \pm 0.05$ g/cm^3, on the local isostatic compensation.

4. Isostatic compensation

Large-scale relief, topography and bathymetry, represent vertical load acting on the lithosphere. The effect of this load is a pushing or flexing of the crust downward into space previously occupied by mantle material. This is referred to as isostasy and is known as Airy isostasy if all compensation occurs immediately below the topographic load (e.g., Watts, 2001). Alternatively, in the Vening Meinesz, or regional isostasy model, the lateral flexural strength of the crust is high enough and distributes the compensation over a wide area (Watts, 2001). The isostatic compensation results in lateral density variations in the lithosphere depths. These density variations are commonly used to calculate the Airy isostatic gravity field. In our study, we examined the Airy isostasy for the constructed lithosphere structure assuming a homogeneous mantle lithosphere. We calculated the expected elevation for the isostatically balanced model without changing the thickness and density of each layer. Subtracting this calculated elevation from the one measured resulted in the residual elevation map. This map indicates compensated and non-compensated regions. After, without changing the crustal structure and its density, we distributed the density in the mantle lithosphere, in order to achieve the Airy isostatic compensation on a regional scale, accounting for the thermal structure of the mantle.

The lithosphere flexure, due to Pliocene–Recent loading and unloading, was calculated for the lithosphere structure obtained with variable densities in the mantle lithosphere. The results of the 3-D gravity modeling and its comparison with the observed gravity field are presented in Section 5. Both the isostasy and gravity numerical modeling carried out using 6×6 km grid nodes enable considering the effects of the regional scale geological features.

4.1. Local isostasy on the Moho level

In this stage, we examined the local isostatic compensation of the 3-D lithosphere structure, assuming a homogeneous mantle lithosphere below the Moho interface. The compensation level is 37 km, the representative

depth to the Moho boundary at the stable and compensated continental Arabian plate (Fig. 2). An average mantle density of 3.25 g/cm^3 is assumed. The resulting calculated elevation differs from the elevation measured on the calculated residual map (Fig. 6A). As the interrelationships between the calculated columns are relative, two geologically stable regions: (A) Jordan on the east; and (B) Egypt on the southwest, were chosen as reference for locally compensatory regions. The calculated elevation significantly deviates from the observed topography in three regions extending over a large part of the area studied. The positive anomaly No. 1 (up to +800 m) on both sides of the Gulf of Elat (Aqaba) probably reflects a low mantle density corresponding to the northward influence of the Red Sea high thermal zone (Ben-Avraham and von Herzen, 1987), which typifies the Red Sea oceanic spreading center. Contrarily, the negative anomaly No. 2 (up to −800 m) in the Herodotus basin suggests a high mantle density reflecting the strong influence of the thickest and coldest lithosphere in the study area. Jimenez-Munt et al. (2003) estimated the lithosphere thickness, which formed during Middle Mesozoic times, is as high as 120 km. The close vicinity of the Cyprus Arc subduction zone may also contribute to this negative anomaly. The highest positive anomaly No. 3 (+1800 m), which is centered in Lebanon and gradually extends southward toward central Israel, can be explained by: (a) error in the constructed crustal structure; (b) non-compensated local isostasy that might have

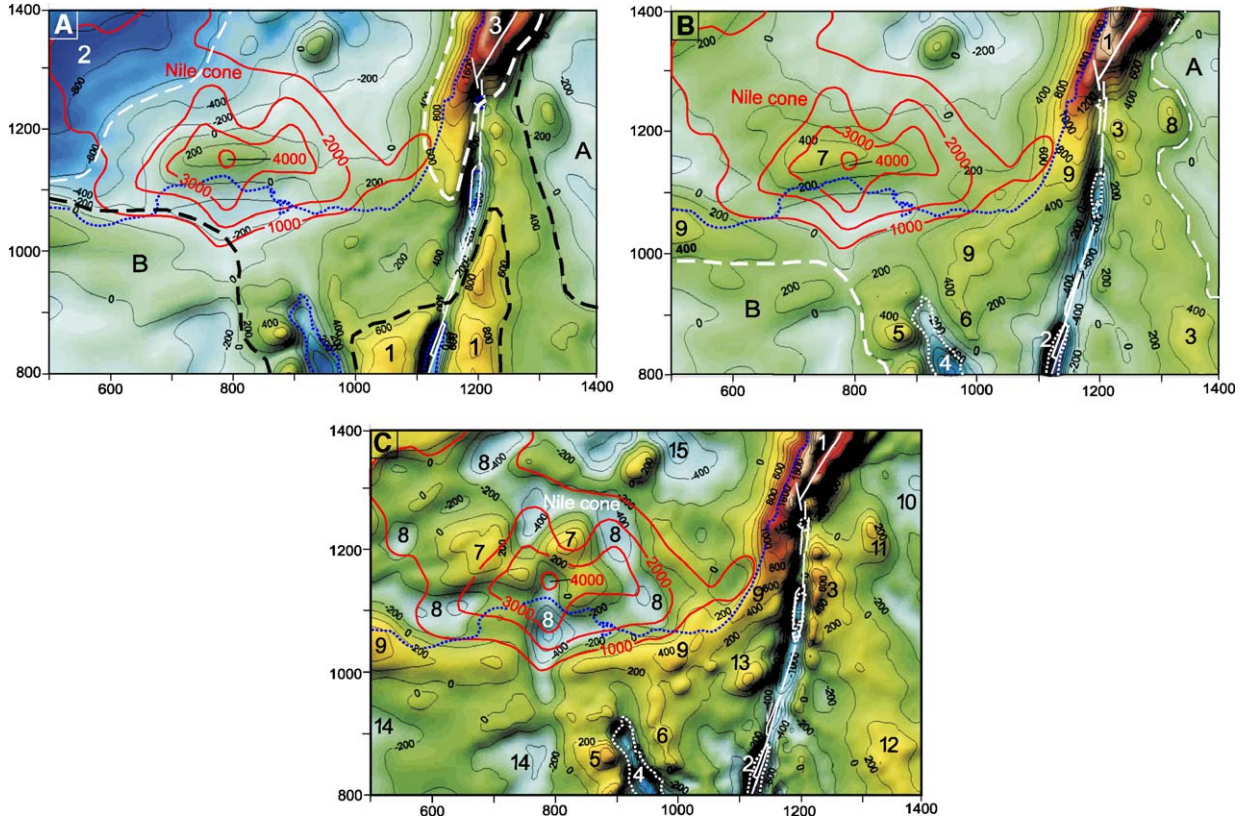

Fig. 6. (A) Residual elevation map calculated by subtracting the calculated elevation, after assuming local (Airy) isostatic compensation on the Moho level (37 km depth), from the measured elevation. Note the location of the regions A and B that are isostatically balanced and regions 1, 2 and 3 which are not balanced. (B) Residual elevation map calculated by subtracting the calculated elevation from the measured one. This calculated elevation assumes local (Airy) isostatic compensation on the base of the lithosphere (100 km depth) and accounts for the density variation in the lithosphere mantle (Fig. 5C). The regions north of the Red Sea and the northern Herodotus basin are now compensated due to the correction in the lithosphere mantle density. The most pronounced anomalies are the positive Lebanon and northern Israel (No. 1) anomaly and the negative anomalies within the tectonic basins along the DST (No. 2) and the Gulf of Suez (No. 4). Moderate positive anomalies are associated with the central (No. 7) and the marginal (No. 9) Nile cone, east of the DST (No. 3) and beside the Gulf of Suez (No. 5, 6). (C) Residual elevation map calculated by subtracting the calculated elevation from the measured one. The calculated elevation assumes flexure isostatic compensation adopting a single rigidity value of $D=10^{23}$ N m, except for the narrow zone representing the DST plate boundary, where $D=10^{16}$ N m is adopted. Most of the area is nearly balanced within the range of ±200 m. The flexure isostasy calculation emphasizes the concentric oscillatory negative and positive anomalies, up to ~400 m high, surrounding the Nile sedimentary cone.

been regionally compensated; (c) density variations in the mantle lithosphere depending upon composition and not temperature; (d) active tectonics.

Examination of the local isostatic compensation suggests that the assumption of a homogeneous lithosphere below the Moho interface is not acceptable. The low density anomaly in the mantle lithosphere around the Gulf of Elat, which matches the positive isostatic anomaly, is supported by petrologic studies on the Arabian plate (Henjes-Kunst, 1989; Altherr et al., 1990; Camp and Roobol, 1992). Furthermore, regional geothermal studies by Pollack et al. (1993) and Jimenez-Munt et al. (2003) suggested thermal variations, and thus density variations, in the mantle lithosphere in the Herodotus basin, a region characterized by negative isostatic anomaly. This evidence and interpretation led us to recalculate the local isostasy, using a deeper compensation level within the mantle lithosphere.

4.2. Local isostasy on lithospheric level at a depth of 100 km

The variations in depth and density of the lithosphere mantle express the uncommon nature of the Levant lithospheric structure, where the continental domain is thinner (~80 km to the base lithosphere) and hotter, as a result of the adjacent Red Sea spreading center. This is in contrast to the cool Mesozoic lithosphere of 100 km deep in most of the oceanic part of the study area. Therefore, a level of compensation at an average depth of 100 km was chosen for recalculating the local isostasy. In order to balance the Red Sea and the Herodotus isostatic anomalies (Fig. 6A), a density variation of $\Delta\rho = \pm 0.05$ g/cm^3, from an average density of 3.25 g/cm^3, was adopted. Thus, the range of the density variations in the lithospheric mantle of the Levant area is between 3.20 and 3.30 g/cm^3 (Fig. 5C). The difference between the calculated and the measured elevations is shown on the residual map (Fig. 6B). These results significantly decrease the previous non-compensated domains, leaving only local anomalies. The most extensive positive anomaly is that of Lebanon and northern Israel (up to +2200 m), which overlaps the weak continental anomaly that is commonly up to +400 m high and causes the arching of central Israel. Only a small positive anomaly (+400 m high) is recorded in the Nile sedimentary cone. An additional weak line of positive anomalies runs SSE from the Sea of Galilee to the Trans Jordan Mountains. The extensive negative anomalies overlap the deep tectonic basins of the DST and the Suez rift (down to −1400 m). The widespread local isostatic compensation was achieved by a small range of densities (±0.05 g/cm^3) in the mantle lithosphere, a fact supporting our suggestion that thermal variations in the mantle lithosphere caused the isostatic anomalies around the Red Sea and the Herodotus basin. The young sedimentary load of the Nile cone and that within the deep tectonic basins along the DST, as well as erosion of high continental terrains, may have a regional effect because of flexural rigidity of the lithosphere. In the following section we present numerical calculations demonstrating a possible effect of the lithosphere flexure.

4.3. Flexure isostasy

The regional (Vening Meinesz) lithosphere response to long-term (>10^6 years) loads has been successfully modeled by a flexure isostasy (e.g., Watts, 2001). Simulations of flexure of an elastic plate with rigidity (D), or effective elastic thickness (T_e), overlying a weak fluid substratum has been used extensively in the oceans and the continents (e.g., Watts, 2001 and references therein) to examine the influence of sedimentary loading or unloading on the topography and the gravity field. Here we present the simulated lithosphere flexure of the study area due to Pliocene–Recent accumulation of the Nile sedimentary cone, basin fill along the DST and the Gulf of Suez, and young basalts, as well as erosion of the continental parts (Fig. 3A). We also calculate the gravity effect related to the lithosphere flexure. An effective elastic thickness of the oceanic lithosphere is usually related to its thermal structure, which is approximately equal to the depth of the 450–600 °C isotherms (e.g., Watts, 2001). The average heat flux in the eastern Mediterranean is about 50 mW/m^2 (Eckstein, 1978; Jimenez-Munt et al., 2003), typical for 80 m.y. of oceanic lithosphere (Parsons and Sclater, 1977) with T_e=25–30 km (e.g., Burov and Diament, 1995, 1996). Tibor et al. (1992) presented a quantitative two-dimensional basin analysis of the late Tertiary Levant passive continental margin along three different cross sections. The results of their modeling show that the elastic thickness in the coastal plain varies across the margin from about T_e=31 km at the base Neogene to about T_e=32 km at the end of the Messinian and slightly decreases seaward. Following the analysis of Tibor et al. (1992), the rigidity value is $D=10^{23}$ N m, corresponding to an elastic thickness of T_e ~30 km. In the flexure isostasy simulations presented in the following section, we adopted this value for the lithosphere of the Levant basin.

The exact physical meaning of T_e for continents is not yet clear and a number of factors, discussed by Burov and Diament (1995, 1996), may significantly reduce the

rigidity value of the continental lithosphere. The regional flexure is a result of the sedimentary loading and unloading. In the model area, during the last 5 m.y., the Nile sedimentary cone is the dominant loading. Additional loading is related to internal sedimentary basins within the DST and the Gulf of Suez fracture systems, which are internal parts of the model (Fig. 3A). The model also accounts for the loading related to the Pliocene volcanics and unloading related to erosion (Fig. 3A). The DST is included in our model as a narrow zone, about 10 km wide, with significantly reduced effective elastic thickness.

The flexure isostatic simulation in the study area, which includes continental margin and plate boundary (DST), has to consider variable effective elastic thickness. In this case the solution for the deflection (w) obtained using the Fourier transform of the loading (e.g., Turcotte and Schubert, 1982) cannot be applied (e.g., Watts, 2001). The differential equation governing the deflection (w) of a thin elastic plate with variable elastic thickness includes additional terms related to the thickness gradients, and hence should be solved using finite difference (Stewart and Watts, 1997) or finite element (van Wees and Cloetingh, 1994) methods. This partial differential equation governing the deflection (w) of a thin elastic plate with variable T_e overlying an inviscid fluid (Stewart and Watts, 1997) is:

$$\rho_l g h = D\nabla\nabla w + 2\frac{\partial D}{\partial x}\frac{\partial}{\partial x}\nabla w + 2\frac{\partial D}{\partial y}\frac{\partial}{\partial y}\nabla w + \nabla D\nabla w - (1-\nu)\left[\frac{\partial^2 D}{\partial x^2}\frac{\partial^2 w}{\partial y^2} - 2\frac{\partial^2 D}{\partial x \partial y}\frac{\partial^2 w}{\partial x \partial y} + \frac{\partial^2 D}{\partial y^2}\frac{\partial^2 w}{\partial x^2}\right] + (\rho_m - \rho_c) g w$$

where g is the gravity acceleration; h is the sediment thickness with density ρ_l; ρ_c is the crustal density; and the rigidity (D) is a function of the effective elastic thickness (T_e), Young modulus ($E \sim 10^{11}$ Pa) and Poisson ratio ($\nu \sim 0.25$) of the elastic plate:

$$D = \frac{E T_e^3(x,y)}{12(1-\nu^2)}$$

Following the methodology presented by Stewart and Watts (1997), we developed a numerical code using a finite difference method to solve the above equation. A linear equation system with a five-diagonal matrix obtained from finite difference discretization is solved by an iteration procedure. Numerical results presented by van Wees and Cloetingh (1994) and Stewart and Watts (1997) were used for benchmarking the code developed.

Several simulations were performed using different values for the rigidity of the continental lithosphere ranging within two orders of magnitude, from $D=10^{22}$ N m to $D=10^{24}$ N m, corresponding to $T_e=20$–60 km. In all simulations a single rigidity value of $D=10^{23}$ N m ($T_e=30$ km) was adopted for oceanic lithosphere. The best match between a modeled flexure and observed elevations (Fig. 6C) is achieved using a single rigidity value of $D=10^{23}$ N m for continental and oceanic lithospheres, except for the narrow fracture zone of the DST. The detailed DST rift structure requires separate treatment in light of its geological configuration. On the one hand, its intensive fracturing indicates weakening, or much lower rigidity; on the other hand, the absence of preferred magmatism within the rift indicates a locking of this plate boundary rather than a free boundary. Gravity evidence also points to a slightly uniform crust across the DST (ten Brink et al., 1999; Hofstetter et al., 2000). This issue was examined by several simulations that led us to use a rigidity value of $D=10^{16}$ N m for the DST internal rift structure. In general, most of the study area is approximately balanced in the range of ±200 m. There is a good match between the outline of the Nile sedimentary cone and the flexure anomalies, indicating their genetic relationships. The central part of the Nile cone yielded a low (~+300 m) positive flexure anomaly, slightly lower than the local residual anomaly. Concentric anomalies, initially negative, followed by positive anomalies up to ~400 m, are associated with the Nile cone and its surroundings. The positive anomaly outside the 1000 m isopach contour of the Nile cone partially overlaps the Lebanon anomaly and continues southwestward toward the northern Negev and northern Sinai, and then westward to Egypt. This anomaly (up to +400 m) may indicate the amount of uplift, or arching, of the Samaria and Judea mountains in central Israel caused by the loading of the Pliocene–Recent sediments of the Nile cone. The distinct positive anomaly in Lebanon (up to +2600 m; [No. 1 on the map]), and southward toward northern Israel (~+1600 m), as well as the distinct negative anomalies of the tectonic basins within the DST [2] and the Gulf of Suez (>−1000 m; [4]), are similar to those obtained by the local isostasy modeling. The positive Lebanon anomaly is situated close to the region (Hula Valley) where the DST branches to several major faults and changes direction from S–N to N30 °E. The flexure anomaly closely follows and parallels the northwestern Yammouneh fault margin (Mount Lebanon), defining its compressional push-up swell character. The high negative anomalies [2] of the Dead Sea and down to the Gulf of Elat are associated with subsidence within tectonic basins caused by pull apart (sort of) basins (e.g., Garfunkel and Ben Avraham, 1996, 2001). The fact that the most intensive residual elevation anomalies of the flexure isostasy are

closely tied to the DST, the major active fault system in the area, point to dynamic power or active tectonics as the fundamental explanation for these anomalies. The loading of Pliocene–Recent sediments within tectonic basins produced these internal negative anomalies [2, 4] and parallel positive anomalies (up to ~600 m; 3, 13, 5 and 6) on the rift margins, depending on the amount of load and the crustal structure. The southward effect of the major positive Lebanon anomaly may have been an additional cause for further arching of central Israel. This explanation is supported by the trend of increasing altitude toward northern Israel and Lebanon.

5. The gravity model

The 3-D gravity model (Fig. 7A) for the layered lithospheric structure was calculated using the PFGRV3D program from "The Potential Field Geophysical Software" (Version 2.0) developed by the U.S. Geological Survey (Cordell et al., 1992). This program calculates a gravity anomaly caused by a source having irregular surfaces, using the Parker–Blakely method (Blakely, 1981). These surfaces are presented as rectangular grids (spacing 6×6 km) that define the top and the bottom of the relevant interfaces. The gravity anomaly of each layer is calculated separately using the differences in density between the model calculated and the Bouguer density (2.67 g/cm^3). This value was found to be optimal by Ginzburg et al. (1993).

The compilation of the observed gravity map utilized a gravity database that was established for the eastern Mediterranean and maritime countries by Rybakov et al. (1997). The database was recently described in detail and supplemented by Rybakov and Al-Zoubi (2005), who used data from the following sources: (1) the Jordanian gravity network; (2) marine gravity measurements of the northeastern part of the Mediterranean Sea south and west of Cyprus; (3) the results of marine gravity surveys in the Israeli offshore; (4) published Bouguer maps of Syria and Egypt; (5) the regional gravity values derived from the Cornell Syria. Database enabled supplementing the regional gravity coverage and filling in gaps in the database for the westernmost part of the study region, the northeastern part of Saudi Arabia and the western part of Iraq (M. Barazangi and his team at the Institute for the Study of the Continents at Cornell University; website at: http://atlas.geo.cornell.edu).

The gravity network contains all the available data and consists of approximately 127,000 data points (Fig. 7B). The data set for the Free air gravity of the region was interpolated to a 6 km cell-size grid by a Kriging algorithm and the map depicted in Fig. 7C.

The Bouguer gravity values were compiled using the 1967 reference ellipsoid and formula with a density of 2.67 g/cm^3 for all the land data. Sea level was taken as the reference datum and the same density (2.67 g/cm^3) was attributed to the water body. In the present framework the gravity data set was interpolated to a 6 km cell-size grid by a Kriging algorithm. The new Bouguer gravity map (Fig. 7D) should be the most reliable gravity map of the study area.

The difference in values (residuals) between the calculated (Fig. 7A) and the observed (Bouguer) gravity (Fig. 7D) is presented also by the same grid spacing of 6×6 km (Fig. 7E). The estimated errors of these calculated gravity values of the dataset for processing (layer geometry and assumed densities) and calculation are negligible. A possible error, corresponding to the inaccuracy factor of the structural interfaces and density estimations, is less than 10 mGal. This value should be taken into account in comparing the observed and the calculated gravity and used as the minimum contour interval for presentation of the calculated gravity and the difference between the observed and the calculated gravity (Fig. 7E). Comparison between the observed (Ginzburg et al., 1993) and the calculated gravity maps shows a similar range and pattern of the total gravity field, between ca. +130 and −90 mGal. This observation is a strong indication that our 3-D structural model for the Levant lithosphere matches the actual subsurface geology of the region. There are two main reasons for the significant differences between the measured and the calculated gravity fields, which are expressed by the residual anomalies: (1) gravity anomalies that occur only on the observed field, such as the positive anomalies in the Mediterranean region (up to +130 mGal; [No. 5 on Fig. 7E]); (2) gravity anomalies that are enhanced by the calculated gravity model, such as the most prominent positive anomaly (up to 140 mGal) of Lebanon and northern Israel [1]. The southwestward continuation of this anomaly, which turns westward [6], surrounding the Nile cone, is only up to ~+30 mGal, and is parallel to the above-mentioned flexure anomaly. The Lebanon and northern Israel high positive gravity anomaly indicates a higher mass that was probably caused by an uplifting of the Moho boundary by dynamic tectonic forces, such as noted for the coexisting flexure anomaly. The exceptional higher positive anomaly west of the central Israel coastline [2] is a result of a positive anomaly on the Bouguer gravity map. Such an anomaly within the Levant continental margins may reflect crustal thinning and rifting, as well as sedimentation and magmatism at the time of their formation. Since this anomaly is centered in the region of the Early

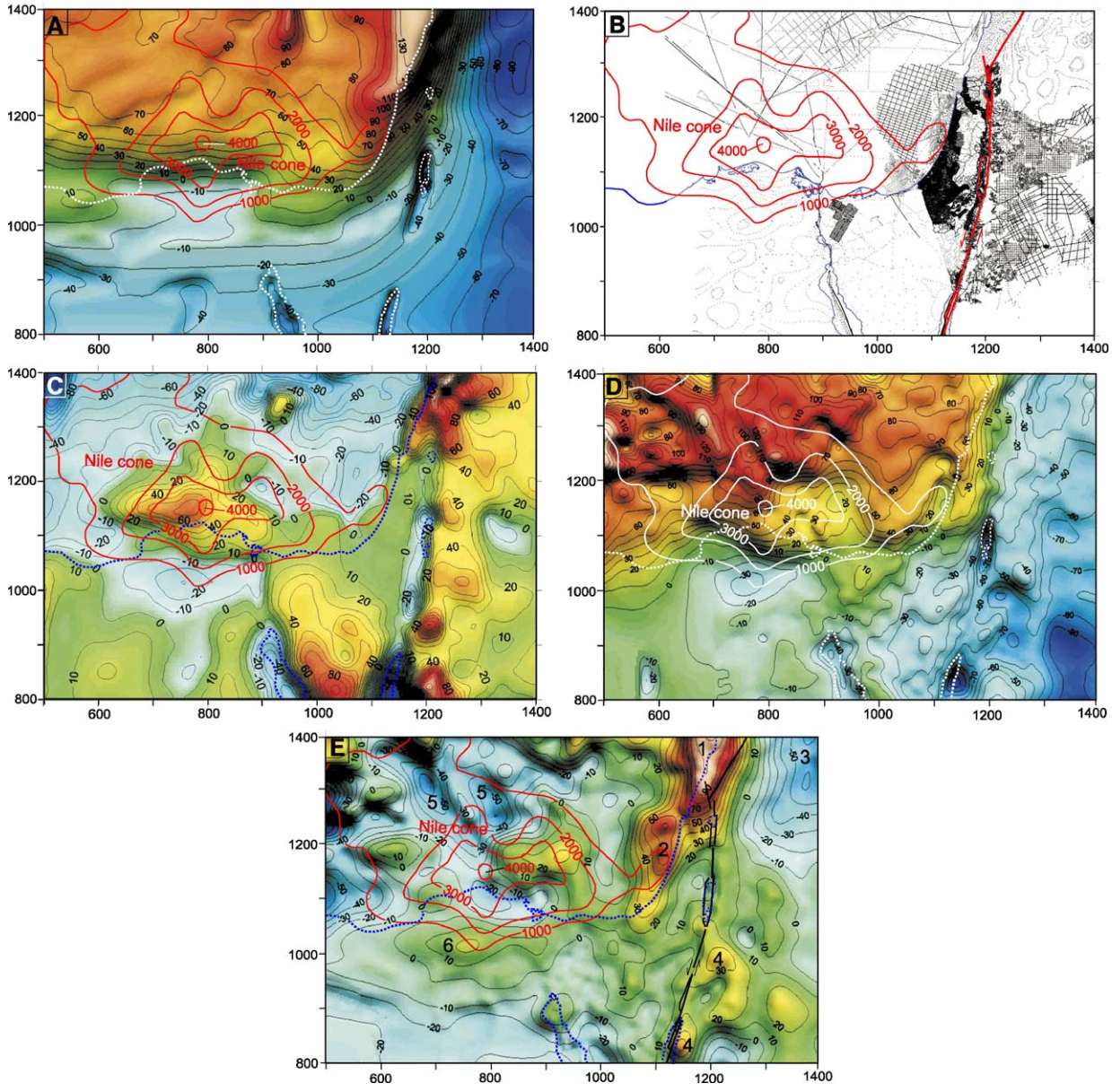

Fig. 7. (A) The calculated Bouguer gravity map (in mGal) for the 3-D lithospheric model described above using variable density values. (B) Gravity coverage map established for the eastern Mediterranean and maritime countries (after Rybakov et al., 1997 and Rybakov and Al-Zoubi, 2005; for details see text). (C) The Free air gravity map (in mGal). Comparing the Free air gravity with the elevation (Fig. 3B), one can recognize the well-known correlation between them except at the southeastern Mediterranean. Here, the positive Free air anomaly coincides well with the thick Nile sedimentary cone. This anomaly also exists in the world scale gravity map derived from ERS-1 Geodetic Mission Altimetry (Knudsen and Andersen, 1995). (D) The Bouguer gravity map (in mGal) after Ginzburg et al. (1993), Rybakov et al. (1997) and Rybakov and Al-Zoubi (2005) and references therein. (E) Residual gravity map calculated by subtracting the observed Bouguer gravity (Fig. 7D) from the calculated gravity (Fig. 7A). The residual gravity in most of the area falls within the range of ±20 mGal, which supports the suggested 3-D lithospheric structure and density distribution in each layer. The possible nature of the strong anomaly in the Lebanese region and several small anomalies are discussed in the text.

Jurassic subsurface Asher volcanics (Gvirtzman and Steinitz, 1983; Kohn et al., 1993), which was situated at the eastern edge of the north Gondwana breakup (Segev, 2000, 2002), it can be explained as a Jurassic magmatic body.

A positive anomaly, up to ~40 mGal, occurs on the eastern margins of the southern DST along the Arava Valley and the Gulf of Elat [4]. This anomaly is evident on the Bouguer gravity field and may indicate the asymmetric topography across the DST (Fig. 2B).

Several negative residual gravity anomalies, up to ~−60 mGal, occur in the Mediterranean region [5]. They occur as elongated positive anomalies on the Bouguer gravity field. Considering the numeric affects for those on the western border of the area studied, there are two distinct northwestward trending elongated anomalies within the Herodotus basin, perpendicular to the nearby Mediterranean ridge. These structures of higher mass may be due to a slightly shallower basement (replacement of sediments by mafic crust) caused by a fault system (horst structures), or dense mafic bodies within the ~11 km sedimentary succession.

The negative anomaly of ~−50 mGal in the NE corner of the study area [3], which occurs on the calculated gravity field, is not clearly understood and may be due to error in the constructed dataset, presumably the grouping of the Jordanian and the Syrian datasets. This means that the Palmyrides and environs, which are interpreted to have about 9–8 km of sedimentary column, may have thinner sedimentary successions.

The modeling presented demonstrate that the calculated gravity field for the constructed regional scale lithosphere structure fits well with the Bouguer gravity field, except for several local geological features that need further detailed investigation.

6. Discussion and conclusions

The 3-D lithospheric structure of the study area emphasizes its main structural elements. The African, Sinai and Arabian continental terrains, which were separated by major fracture systems (the DST and the Suez rift), reach their maximal thickness (37 km) in the Arabian plate. The Levant and Herodotus marine basins, which are separated by the Eratosthenes Seamount (a small continental fragment, according to Makris et al., 1983; Ben Avraham et al., 2002), has a crustal thickness of ~23 km, of which ~9 km are sediments. The lithosphere structure of the study area is based on the interpretations of seismic measurements and borehole data. Based on these interpretations the crust of the Levant basin is suggested to be oceanic. The oceanic nature of the crust is supported by the present study that compares gravity modeling with observations and demonstrates that most of the Levant basin is isostatically compensated. Moreover, the alternative possibility of thin continental crust beneath the Levant basin would decrease the average crustal density from 2.9 to 2.8 g/cm^3 (Fig. 5B) and, hence, would change the simulated gravity by more than 50 mGal. In addition, such a thin continental crust beneath the Levant basin cannot be isostatically compensated and would elevate the whole Levant basin by more than 400 m. The oceanic nature of the Levant basin implies that the age of the sedimentary rocks is younger than Jurassic, the suggested time for the formation of this basin.

Our dataset emphasizes the structure in the region of the Nile cone, where a thick Pliocene–Recent sedimentary prism accumulated on the top of mobile Messinian evaporates. The thickness of the Nile sediments is inversely well correlated with the thickness of the pre-Pliocene sedimentary succession, down to the top of the crystalline basement. The relatively flat bathymetry and flat relief of the crystalline basement cause this relation, which is also supported by several geophysical studies (e.g., Said, 1981; Abdel Aal et al., 2000; Loncke et al., 2002; Gaullier et al., 2002). They found structures typical to gravity-driven spreading and gliding of the mobile salt layer (salt tectonics) below the Nile cone. Lateral flow of evaporates cause a thinning of the salt deposits below the central part of the cone and an outward thickening up to 2.8 km (e.g., Loncke et al., 2002) of the evaporates as diapirs, salt walls and buckle folds (Costa and Vendeville, 2002). Garfunkel and Almagor (1985) discussed the salt tectonics recently recognized by Martinez et al. (2005) and its impact on the sediments offshore Israel. Similar salt tectonic features have been observed in the Rhône deep-sea fan (Gaullier and Bellaiche, 1996; Gaullier et al., 2002), Gulf of Lions and Ebro within the Mediterranean Sea (Loncke et al., 2002), along the Atlantic margin, i.e., North Sea, Nigeria, Angola, Gulf of Mexico (Worrall and Snelson, 1989) and other regions.

The lithosphere structure presented here was first examined for local isostatic compensation on the Moho level and the calculations show significant deviations from the isostasy. Moving the compensation level to a 100 km depth and adopting density variations in the mantle lithosphere in the range of ±0.05 g/cm^3, in agreement with a regional heat flux, yielded isostatic compensation over most of the area studied. The common deviations from the local isostasy are less than ±500 m. The Levant basin having oceanic crust was found to be compensated. An alternative possibility to achieve local isostasy with homogeneous density of the mantle lithosphere leads to significant change of the crustal thickness, contradicting the seismic evidence. The final compensated 3-D lithosphere structure of the study area yielded several residual elevation anomalies, as follows:

- A high positive anomaly found in Lebanon and northern Israel means that the elevation measured in this terrain is much higher than that calculated from the isostatic considerations. The reasons can be: active tectonics leading to dynamic forces in the crust or the mantle; variations in density caused by variations in

composition not accounted for in the lithosphere structure presented; error in the database.

- High negative anomalies are found in the DST tectonic basins and the southern Gulf of Suez, which means that these basins tend to subside in environments without tectonic stress, or they reflect uncertainties or too wide spacing of the grid nodes.
- Low positive anomalies (up to 400 m) are located: (1) in the Nile sedimentary cone; (2) along the continental margin, along the central Israel N–S mountain ranges (arching) and northern Sinai; and (3) from the Sea of Galilee toward the SSE.
- A low positive anomaly (~600 m) is located west of the Gulf of Suez.

Simulations of flexure isostasy related to the Pliocene–Recent sedimentary loading and unloading due to erosion (Fig. 3A) improves the compensation of the area, keeping the general pattern of the anomalies similar to the local isostasy. The complexity of the study area and lack of detailed density data does not enable constraining the effective elastic thickness well. The flexure rigidity of the Levant continental and the oceanic lithospheres (Arabian, Sinai and NE African plates) is suggested to be $D=10^{23}$ N m, whereas the rigidity for the DST plate boundary is $D=10^{16}$ N m. The model with this rigidity value provides the best match with the observed elevation. A similar single T_e value, about 30–40 km, for both continental and oceanic lithospheres has been suggested for the Atlantic margin of North America (Fig. 6.30 in Watts, 2001). Both passive margins are of the same Jurassic age (Segev, 2000, 2002).

Similar to the local isostasy, the largest positive anomaly is located in Lebanon and northern Israel, mainly between the Yammouneh fault and the Lebanese coastline, the region where compressional push-up tectonic structures are usually presumed. The high negative anomalies associated with the DST tectonic basins are probably the result of subsidence within dynamic pull-apart (sort of) structures.

The loading of the Nile sedimentary cone since the Pliocene yielded a low positive anomaly (up to +300 m) within its center, which is surrounded by concentric oscillatory negative and positive anomalies, up to ~400 m high. The negative anomaly in the Levant basin, close to the 2000 m isopach contour of the Nile cone, may explain the Pliocene subsidence "anomaly" near Israel reported by Tibor et al. (1992). Moreover, the positive anomaly outside the 1000 m isopach contour of the Nile cone located on the continental part in central Israel, northern Sinai and Egypt may indicate the reason for the arching of this region (e.g., Picard, 1951; Wdowinski and Zilberman, 1997). Both features, the subsidence and arching of about ±400 m, are similar to the flexure anomalies.

Gravity modeling of the 3-D lithospheric structure established herein, having variable horizontal and vertical densities, provided an independent constraint for the large scale lithospheric structure and emphasized the following small-scale residual anomalies:

- The general agreement between the calculated gravity and the observed (Bouguer) one is the major constraint on the 3-D lithosphere structure suggested herein and on the composition of the Levant and the southeastern Mediterranean area, including the oceanic nature of the Levant basin.
- The Lebanon and northern Israel high positive gravity residual anomaly, which is caused by an elevated mantle lithosphere, also points to a compressional push-up mechanism for this region.
- The positive anomaly west of the central Israel coastline may reflect a Jurassic magmatic (Asher volcanics) body, associated rifting and continental breakup in the Levant marine basin. The concentric low gravity anomalies of the Nile sedimentary cone were discussed above.
- The northwestward trending elongated gravity (positive Bouguer) anomalies in the Herodotus basin represent structures of higher mass probably due to a basin-and-swell fault system.
- The negative anomaly in the NE corner of the study area is probably an artifact in the dataset.

Acknowledgments

Discussions with R. Weinberger and Z. Gvirtzman were greatly appreciated. We thank Hans Thybo (editor), J. Ebbing and J.C. Mareschal for their constructive reviews, and B. Katz for editing the text. The study was partially supported by a grant from the US–Israel Binational Science Foundation (BSF), Jerusalem, Israel (2004946) to A. Segev and V. Lyakhovsky.

References

Abdel Aal, A., El Barkooky, A., Gerrits, M., Meyer, H., Schwander, M., Zaki, H., 2000. Tectonic evolution of the Eastern Mediterranean basin and its significance for hydrocarbon prospectivity in the ultra deep water of the Nile Delta. Lead. Edge 19 (10), 1086–1102.

Al-Husseini, M.I., 1997. Jurassic sequence stratigraphy of the western and southern Arabian Gulf. GeoArabia 2 (4), 361–382.

Aldersons, F., Ben-Avraham, Z., Hofstetter, A., Kissling, E., Al-Yazjeen, T., 2003. Lower crustal strength under the Dead Sea basin from local earthquake data and rheological modeling. Earth Planet. Sci. Lett. 214, 129–142.

Altherr, R., Henjes-Kunst, F., Baumann, A., 1990. Asthenosphere versus lithosphere as possible sources for basaltic magmas erupted during formation of the Red Sea: constraints from Sr, Pb and Nd isotopes. Earth Planet. Sci. Lett. 96, 269–286.

Avni, Y., 1998. Paleogeography and tectonics of the central Negev and the Dead Sea rift western margin during the Late Neogene and Quaternary. Isr. Geol. Surv. Rep. GSI/24/98, 231 p. (Ph.D. Thesis, Hebrew Univ., Jerusalem; in Hebrew with English abstract).

Badri, M., Sayer, C.M., Awad, R., Graziano, A., 2000. A feasibility study for porepressure prediction using seismic velocities in the offshore Nile delta, Egypt. Lead. Edge 19; 10, 1103–1104, 1106–1108.

Batayneh, A.T., Al Zoubi, A.S., 2001. The gravity field and crustal structure of the northwestern Arabian platform in Jordan. J. Afr. Earth Sci. 32 (1), 141–148.

Begin, Z.B., Zilberman, E., 1997. Main stages and rates of relief development in Israel. Isr. Geol. Surv. Rep. (GSI/24/97, 63 p).

Bellaiche, G., Loncke, L., Gaullier, V., Droz, L., Mascle, J., Courp, T., Moreau, A., Radan, S., Sardon, O., 2002. The Nile deep-sea fan and its channel-levees system. PRISMED II and FANIL Cruises. CIESM Workshop Ser. 17, 49–53.

Ben Avraham, Z., 1985. Structural framework of the Gulf of Elat (Aqaba), northern Red Sea. J. Geophys. Res. 90 (B1), 703–726.

Ben Avraham, Z., Mart, Y., 1981. Late Tertiary structure and stratigraphy of north Sinai continental margin. Am. Assoc. Pet. Geol. Bull. 65, 1135–1145.

Ben-Avraham, Z., von Herzen, R.P., 1987. Heat flow and continental breakup: the Gulf of Elat (Aqaba). J. Geophys. Res. 92, 1407–1416.

Ben Avraham, Z., Hanel, R., Villinger, H., 1978. Heat flow through the Dead Sea rift. Mar. Geol. 28, 253–269.

Ben Avraham, Z., Tibor, G., Limonov, A.F., Leybov, M.B., Ivanov, M.K., Tokarev, M.Y., Woodside, J.M., 1995. Structure and tectonics of the eastern Cyprean Arc. Mar. Pet. Geol. 12 (3), 263–271.

Ben Avraham, Z., ten Brink, U., Bell, R., Reznikov, M., 1996. Gravity field over the Sea of Galilee: evidence for a composite basin along the transform fault. J. Geophys. Res. 101 (B1), 533–544.

Ben Avraham, Z., Ginzburg, A., Makris, J., Eppelbaum, L., 2002. Crustal structure of the Levant Basin, eastern Mediterranean. Tectonophysics 346 (1–2), 23–43.

Bentor, Y.K., Vroman, A.J., 1960. Geological Map of Israel, 1:100,000, Sheet 16: Mount Sdom. Isr. Geol. Surv., 117 p., 2nd ed.

Best, J.A., Barazangi, M., Al-Saad, D., Sawaf, T., Gebran, A., 1990. Bouguer gravity trends and crustal structure of the Palmyride mountain belt and surrounding northern Arabian platform in Syria. Geology 18, 1235–1239.

Blakely, R.J., 1981. A program for rapidly computing the magnetic anomaly over digital topography. U.S. Geol. Surv. Open-File Rep. 81–298 (46 p.).

Brian, M.W., 1998. Subsidence record of early-stage continental collision, Eratosthenes platform (Sites 966 and 967). In: Robertson, A.H.F., Emeis, K.C., Richter, C., Camerlenghi, A. (Eds.), Proceedings of the Ocean Drilling Program, vol. 160, pp. 509–515.

Burollet, P., Gennesseaux, M., 1998. Plio–Quaternary isopach map (IBCM-PQ). IBCM Geological–Geophysical Series, Mercator projection, scale 1:1,000,000 at 38°N latitude, 10 sheets with 200 m isopach contours borehole designations, and structural interpretations. Intergovern. Oceanog. Comm. (IOC–UNESCO) (Final Version) Head Department of Navigation and Oceanography, Ministry of Defence, St. Petersburg, Russian Federation.

Burov, E.B., Diament, M., 1995. The effective elastic thickness (T_e) of continental lithosphere: what does it really mean? J. Geophys. Res. 100, 3905–3927.

Burov, E.B., Diament, M., 1996. Isostasy, equivalent elastic thickness, and inelastic rheology of continents and oceans. Geology 24, 419–422.

Calvo, R., 2002. Stratigraphy and petrology of the Hazeva Formation in the Arava and the Negev: Implications for the development of sedimentary basins and the morphotectonics of the Dead Sea Rift Valley. Isr. Geol. Surv. Rep. GSI/22/02, 264 p. (Ph.D. Thesis, Hebrew Univ., Jerusalem; in Hebrew with English abstract).

Camp, V.E., Roobol, M.J., 1992. Upwelling asthenosphere beneath western Arabia and its regional implications. J. Geophys. Res., B11, 15,255–15, 271.

Cordell, L., Phillips, J.D., Godson, R.H., 1992. U.S. Geological Survey Potential Field Geophysical Software, Version 2.0. Department of the Interior, U.S. Geological Survey.

Costa, E., Vendeville, B.C., 2002. Experimental insights on the geometry and kinematics of fold-and-thrust belts above weak, viscous evaporitic decollement. J. Struct. Geol. 24 (11), 1729–1739.

Courtillot, V., Armijo, R., Tapponnier, P., 1987. The Sinai triple junction revisited. Tectonophysics 141, 181–190.

DESERT Group, Weber, M., et al., 2004. The crustal structure of the Dead Sea Transform. Geophys. J. Int. 156, 655–681, doi:10.1111/j.1365-246X.2004.02143.x.

Druckman, Y., Gvirtzman, G., Kashai, E., 1975. Distribution and environment of deposition of Upper Triassic on the northern margins of the Arabian Shield and around the Mediterranean Sea. Proc IXth Intern. Cong. Sedimentology, Nice, Theme, 5, 1, pp. 183–192.

Eckstein, Y., 1978. Review of heat flow data from the Eastern Mediterranean region. Pure Appl. Geophys. 117 (1/2), 150–159.

El-Isa, Z., Mechie, J., Prodehl, C., Makris, J., Rihm, R., 1987. A crustal structure study of Jordan derived from seismic refraction data. Tectonophysics 138, 235–253.

Evans, A.L., 1988. Neogene tectonic and stratigraphic events in the Gulf of Suez rift area, Egypt. Tectonophysics 153, 235–247.

Eyal, M., Eyal, Y., Bartov, Y., Steinitz, G., 1981. The tectonic development of the western margin of the Gulf of Elat (Aqaba) rift. Tectonophysics 80, 39–66.

Feinstein, S., Kohn, B.P., Steckler, M.S., Eyal, M., 1996. Thermal history of the eastern margin of the Gulf of Suez, 1. Reconstruction from borehole temperature and organic maturity measurements. Tectonophysics 266, 203–220.

Freund, R., Garfunkel, Z., Zak, I., Goldberg, M., Weissbrod, T., Derin, B., 1970. The shear along the Dead Sea rift. Philos. Trans. R. Soc. Lond. A 267, 107–130.

Frieslander, U., 2000. The structure of the Dead Sea Transform emphasizing the Arava using new geophysical data. Ph.D. Thesis, The Hebrew Univ. Jerusalem, 101 p. (in Hebrew with English abstract).

Garfunkel, Z., 1981. Internal structure of the Dead Sea leaky transform (rift) in relation to plate kinematics. Tectonophysics 80, 81–108.

Garfunkel, Z., 1998. Constraints on the origin and history of the Eastern Mediterranean basin. Tectonophysics 298, 5–35.

Garfunkel, Z., Almagor, G., 1985. Geology and structure of the continental margin of northern Israel and the adjacent part of the Levantine Basin. Mar. Geol. 62, 105–131.

Garfunkel, Z., Bartov, Y., 1977. The tectonics of the Suez rift. Isr. Geol. Surv. Bull. 71 44 p.

Garfunkel, Z., Ben Avraham, Z., 1996. The structure of the Dead Sea Basin. Tectonophysics 266, 155–176.

Garfunkel, Z., Ben Avraham, Z., 2001. Basins along the Dead Sea transform. Peri Tethys Mem. 6: Peri Tethyan rift/wrench basins and passive margins. In: Ziegler, P.A., et al. (Eds.), Mus. Natl. Hist. Nat., Mem., vol. 186, pp. 607–627.

Garfunkel, Z., Horowitz, A., 1966. The upper Tertiary and the Quaternary morphology of the Negev. Isr. J. Earth Sci. 15, 101–117.

Gaullier, V., Bellaiche, G., 1996. Ligurian–Provencal diapirism; the effects of residual topography below the Messinian salt decollement; insights from analog modelling. Comptes Rendus de l'Academie des Sciences, Ser. II. Sci. Terre Planet 322 (3), 213–220.

Gaullier, V., Loncke, L., Vendeville, B.C., Mascle, J., Maillard, A., 2002. Salt tectonics in the Nile and Rhône deep-sea fans: comparison on the basis of seismic data and physical modeling. CIESM Workshop Ser. 17, 39–42.

Gennesseaux, M., Burollet, P., Winnock, E., 1998. Thickness of the Plio–Quaternary sediments (IBCM-PQ). Boll. Geofis. Teor. Appl. 39 (4), 243–284.

Giannérini, G., Campredon, R., Féraud, G., Abou Zakhem, B., 1988. Déformations intraplaques et volcanisme associé: exemple de la bordure NW de la plaque Arabique au Cénozoïque. Bull. Soc. Géol. Fr. 4 (6), 937–947.

Ginzburg, A., Ben Avraham, Z., 2001. Geophysics. In: Horowitz, A. (Ed.), The Jordan Rift Valley. Balkema Publishers, Lisse/Abingdon/Exton(PA)/Tokyo, pp. 369–421.

Gvirtzman, G., Steinitz, G., 1983. The Asher volcanics — an Early Jurassic event in northern Israel. Isr. Geol. Surv. Curr. Res. 3, 28–33.

Ginzburg, A., Cohen, S.S., Hay-Roen, H., Rosenzweig, A., 1975. Geology of Mediterranean shelf of Israel. Am. Assoc. Pet. Geol. Bull. 59, 2142–2160.

Ginzburg, A., Makris, J., Fuchs, K., Prodehl, C., Kaminski, W., Amitai, U., 1979. A seismic study of the crust and upper mantle of the Jordan–Dead Sea rift and their transition toward the Mediterranean Sea. J. Geophys. Res. 84, 1569–1582.

Ginzburg, A., Folkman, Y., Rybakov, M., Rotstein, Y., Assael, R., Yuval, Z., 1993. Bouguer gravity map of Israel and adjacent areas (1:500,000). Inst. Petrol. Res. Geophy. (Geophy. Res. Inst. Isr.), map.

Heimann, A., 1990. The development of the Dead Sea Rift and its margins in northern Israel during the Pliocene and the Pleistocene. Isr. Geol. Surv. Rep. (GSI/28/90, 114 p. in Hebrew, English abstract).

Heimann, A., Steinitz, G., Mor, D., Shaliv, G., 1996. The Cover Basalt Formation, its age and its regional and tectonic setting: implication from K–Ar and $^{40}Ar/^{39}Ar$ geochronology. Isr. J. Earth Sci. 45, 55–71.

Henjes-Kunst, F., 1989. Mantle xenoliths in western Arabia and their bearing on asthenosphere–lithosphere dynamics during formation of the Red Sea Rift — a review. Spannung und Spannungsumwandlung in der Lithosphare, Symposium on the Afro-Arabian Rift System. Karlsruhe University, Karlsruhe, Germany, pp. 49–50.

Hirsch, F., Flexer, A., Rosenfeld, A., Yellin-Dror, A., 1995. Palinspastic and crustal setting of the eastern Mediterranean. J. Pet. Geol. 18 (2), 149–170.

Hirsch, F., Bassoullet, J.P., Cariou, E., Conway, B., Feldman, H.R., Grossowicz, L., Honigstein, A., Owen, E.F., Rosenfeld, A., 1998. The Jurassic of the southern Levant. Biostratigraphy, palaeogeography and cyclic events. In: Crasquin-Soleau, S., Barrier, E. (Eds.), Peri-Tethys Memoir 4: Epicratonic Basins of Peri-Tethyan Platforms. Mém. Mus. Natn. Hist. Nat., vol. 179, pp. 213–235.

Hofstetter, A., Bock, G., 2004. Shear-wave velocity structure of the Sinai sub-plate from Receiver Function analysis. Geophys. J. Int. 158, 67–84.

Hofstetter, A., Dorbath, C., Rybakov, M., Goldshmidt, V., 2000. Crustal and upper mantle structure across the Dead Sea rift and Israel from teleseismic P wave tomography and gravity data. Tectonophysics 327, 37–59.

Hofstetter, A., Feldman, L., Rotstein, Y., 1991. Crustal structure of Israel; constraints from teleseismic and gravity data. Geophys. J. Int. 104 (2), 371–379.

Hsu, K.J., Montadert, L., Bernoulli, D., Cita, M.B., Erickson, A., Garrison, R.E., Kidd, R.B., Melieres, F., Muller, C., Wright, R., 1977. History of the Mediterranean salinity crisis. Nature 267, 399–403.

Ilani, S., Harlavan, Y., Tarawneh, K., Rabba, I., Weinberger, R., Ibrahim, K., Peltz, S., Steinitz, G., 2001. New K–Ar ages of basalts from the Harrat Ash Shaam volcanic field in Jordan: implications for the span and duration of the upper-mantle upwelling beneath the western Arabian plate. Geology 29 (2), 171–174.

Jimenez-Munt, I., Sabadini, R., Gardi, A., Bianco, G., 2003. Active deformation in the Mediterranean from Gibraltar to Anatolia inferred from numerical modeling and geodetic and seismological data. J. Geophys. Res. 108 (B1), 2006, doi:10.1029/2001JB001544.

Klitzsch, E., 1991. Geological observations from Nubia and their structural interpretation. In: Salem, M.J., Busrewil, M.T., Ashour, A.M. (Eds.), The Geology of Libya, vol. VII, pp. 101–105.

Kohn, B.P., Lang, B., Steinitz, G., 1993. $^{40}Ar/^{39}Ar$ dating of the Atlit-1 volcanic sequence, northern Israel. Isr. J. Earth Sci. 42, 17–28.

Knudsen, P., Andersen, O.B., 1995. Global Gravity Anomalies from ERS-1 Altimetry, Geodetic Mission (168 days). Ocean Gravity Map 1:48,000,000 at the Equator, Kortog Matrikeistyrelsen, Copenhagen, Denmark.

Lartet, M.L., 1869. Essai sur la geologie de la Palestine et des contrees avoisinantes. Ann. Sci. Geol. 1, 5–116.

Limonov, A.F., Limonova, I.V., Gennesseaux, M., 1992. Levantine Sea Plio–Quaternary sediment thickness. In: Gennesseaux, M., Winnock, E. (Eds.) (1993). Thickness of the Plio–Quaternary sediments. Intergovernmental Oceanographic Commission (UNESCO) IBCM Geol. Geophys. Ser., Scale 1:1 000 000, 10 Sheets, St. Petersburg.

Loncke, L., Gaullier, V., Mascle, J., Vendeville, B., 2002. Shallow structure of the Nile deep-sea fan. Interactions between structural heritage and salt tectonics; consequences on sedimentary dispersal. CIESM Workshop Ser. 17, 43–48.

Lort, J.M., 1973. Summary of seismic studies in the eastern Mediterranean. Geol. Soc. Greece Bull. 10 (1), 99–108.

Lort, J.M., Limond, W.Q., Gray, G., 1974. Preliminary seismic studies in the eastern Mediterranean. Earth Planet. Sci. Lett. 21, 355–366.

Makris, J., Ben-Abraham, Z., Behle, A., Ginzburg, A., Giese, A., Steinmetz, I., Whitmarsh, R.B., Eleftheriou, S., 1983. Seismic refraction profiles between Cyprus and Israel and their interpretation. Geophys. J. R. Astron. Soc. 75, 575–591.

Makris, J., Wang, J., 1994. Bouguer gravity anomalies of the eastern Mediterranean Sea. In: Krasheninnikov, V.A., Hall, J.K. (Eds.), Geological Structure of the Northeastern Mediterranean (Cruise 5 of the research vessel 'Akademik Nikolaj Strakhov'), Jerusalem, pp. 87–98.

Marcus, E., Slager, J., 1985. The sedimentary–magmatic sequence of the Zemah 1 Well (Jordan Dead Sea Rift, Israel) and its emplacement in time and place. Isr. J. Earth Sci. 34, 1–10.

Mart, Y., Eisin, B., 1982. Some faulting patterns along the continental margin of the NE Mediterranean. Mar. Geophys. 5, 249–262.

Martinez, J.F., Cartwright, J., Hall, B., 2005. 3D seismic interpretation of slump complexes: examples from the continental margin of Israel. Basin Res. 17, 83–108.

Mascle, J., Benkheli, J., Bellaiche, G., Zitter, T., Woodside, J., Loncke, L., Prismed II Scientific Party, 2000. Marine geological evidence for the Levantine–Sinai plate, a new piece of the Mediterranean puzzle. Geology 28, 779–782.

Matmon, A., Wdowinski, S., Hall, J.K., 2003. Morphological and structural relations in the Galilee extensional domain, northern Israel. Tectonophysics 371, 223–241.

Maurath, G., Eckstein, Y., 1990. Using heat flow models to delineate timing of tectonic movement along the Jordan/Dead Sea transform. Geol. Soc. Am. 22 (7), 154 (abstract).

McGuire, A.V., Bohannon, R.G., 1989. Timing of mantle upwelling: evidence for a passive origin for the Red Sea rift. J. Geophys. Res. 94, 1677–1682.

McKenzie, D.P., Davies, D., Molnar, P., 1970. Plate tectonics of the Red Sea and East Africa. Nature 226, 243–248.
Parsons, B.E., McKenzie, D.P., 1978. Mantle convection and the thermal structure of plates. J. Geophys. Res. 83, 4485–4496.
Parsons, B., Sclater, J.G., 1977. An analysis of the variation of ocean floor bathymetry and heat flow with age. J. Geophys. Res. 82 (5), 803–827.
Patton, T.L., Moustafa, A.R., Nelson, R.A., Abdine, A.S., 1994. Tectonic evolution and structural setting of the Suez rift. In: London, S.M. (Ed.), Interior Rift Basins. AAPG Mem., vol. 58, pp. 9–55.
Picard, L., 1951. Geomorphogeny of Israel, 1. The Negev. Res. Counc. Bull. 8G, 1–30.
Picard, L., 1966. Thoughts on the graben systems of the Near East. Pap. Geol. Surv. Can. 66 (14), 22–34.
Pollack, H.N., Hurter, S.J., Johnson, J.R., 1993. Heat loss from the Earth's interior: analysis of the global data set. Rev. Geophys. 31, 267–280.
Poudjom Djomani, Y.H., O'Reilly, S.Y., Griffin, W.L., Morgan, P., 2001. The density structure of subcontinental lithosphere through time. Earth Planet. Sci. Lett. 184, 605–621.
Ross, D.A., Uchupi, E., 1977. Structure of sedimentary history of southeastern Mediterranean sea–Nile cone area. Am. Assoc. Pet. Geol. Bull. 61, 872–902.
Ryan, W.B.F., Cita, M.B., 1978. The nature and distribution of Messinian erosional surfaces—indicators of a several-kilometer-deep Mediterranean in the Miocene. Mar. Geol. 27, 193–230.
Rybakov, M., Al-Zoubi, A., 2005. Bouguer Gravity Map of the Levant — A New Compilation. In: Hall, J.K., Krasheninnikov, V.A., Hirsch, F., Benjamini, C.H., Flexer, A. (Eds.), Geological Framework of the Levant, Volume II: The Levantine Basin and Israel. Historical Productions-Hall, Jerusalem, pp. 539–542. Chapter 19.
Rybakov, M., Segev, A., 2004. Top of the crystalline basement in the Levant. Geochem. Geophys. Geosyst. 5, doi:10.1029/2004GC000690.
Rybakov, M., Goldshmidt, V., Rotstein, Y., 1997. New regional gravity and magnetic maps of the Levant. Geophys. Res. Lett. 24 (1), 33–36.
Rybakov, M., Goldshmidt, V., Rotstein, Y., Fleischer, L., Goldberg, I., 1999. Petrophysical constraints on gravity/magnetic interpretation in Israel. Lead. Edge 18 (2), 269–272.
Sahagian, D.L., 1993. Structural evolution of African Basins: stratigraphic synthesis. Basin Res. 5, 41–54.
Said, R., 1981. The Geological Evolution of the River Nile. Springer, New York. 151 p.
Salamon, A., 1987. The monoclines in the northern Negev: a model of tilted blocks and shortening. M.Sc. Thesis, Hebrew Univ., Jerusalem (in Hebrew with English abstract), 101 p.
Seber, D., Vallve, M., Sandvol, E., Steer, D., Barazangi, M., 1997. Middle East tectonics: applications of geographic information system. Geol. Soc. Am. Today 7 (2), 1–6.
Segev, A., 2000. Synchronous magmatic cycles during the fragmentation of Gondwana: radiometric ages from the Levant and other provinces. Tectonophysics 325 (4), 257–277.
Segev, A., 2002. Flood basalts, continental breakup and the dispersal of Gondwana: evidence for periodic migration of upwelling mantle flows (plumes). Eur. Geosci. Uni., Stephan Mueller Spec. Publ. Ser., vol. 2, pp. 171–191.
Segev, A., Goldshmidt, V., Rybakov, M., 1999. Late Precambrian–Cambrian tectonic setting of the crystalline basement in the northern Arabian–Nubian Shield as derived from gravity and magnetic data: Basin-and-range characteristics. Isr. J. Earth Sci. 48, 159–178.
Shaliv, G., 1991. Stages in the tectonic and volcanic history of the Neogene basin in the Lower Galilee and the valleys. Isr. Geol. Surv. Rep., GSI/11/91, (Ph.D. Thesis, in Hebrew, English abstract), 94 p.
Sneh, A., 1996. The Dead Sea Rift: lateral displacement and downfaulting phases. Tectonophysics 263, 277–292.
Sneh, A., 1999. Cross-rift drainage system successions in the Hazeva Formation (Miocene), Dead Sea Rift area, Israel. Isr. J. Earth Sci. 48, 247–256.
Steckler, M.S., Feinstein, S., Kohn, B.P., Lavier, L.L., Eyal, M., 1998. Pattern of mantle thinning from subsidence and heat flow measurements in the Gulf of Suez: evidence for the rotation of Sinai and along-strike flow from the Red Sea. Tectonics 17, 903–920.
Stewart, J., Watts, A.B., 1997. Gravity anomalies and spatial variations of flexural rigidity at mountain ranges. J. Geophys. Res. 102, 5327–5352.
ten Brink, U.S., Schoenberg, N., Kovach, R., Ben Avraham, Z., 1990. Uplift and a possible Moho offset across the Dead Sea transform. Tectonophysics 180, 71–85.
ten Brink, U.S., Rybakov, M., Al-Zoubi, A.S., Hassouneh, M., Frieslander, U., Batayneh, A., Goldschmidt, V., Daoud, M.N., Rotstein, Y., Hall, J.K., 1999. Anatomy of the Dead Sea transform: does it reflect continuous changes in plate motion? Geology 27, 887–890.
Tibor, G., Ben Avraham, Z., Steckler, M., Fligelman, H., 1992. Late Tertiary subsidence history of the southern Levant margin and its implications to the Messinian event. J. Geophys. Res. 97, 17,593–17,614.
Tibor, G., Lyakhovsky, V., Ben Avraham, Z., Achmon, M., Fligelman, H., 1993. The regional effects of the Nile delta load on the vertical movements of the Levant continental margin since the Pliocene. The Ministry of Energy and Infrastructures Rep. ES-26-93. 16 pp.
Turcotte, D.L., Schubert, G., 1982. Geodynamics: Application of Continuum Physics to Geological Problems. John Wiley, Hoboken, N.J.
van Wees, J.D., Cloetingh, S., 1994. A finite-difference technique to incorporate spatial variations in rigidity and planar faults into 3-D models of lithospheric flexure. Geophys. J. Int. 117, 199–195.
Watts, A.B., 2001. Isostasy and Flexure of the Lithosphere. Cambridge Univ. Press. 458 pp.
Wdowinski, S., Zilberman, E., 1997. Systematic analyses of the large-scale topography and structure across the Dead Sea Rift. Tectonics 16 (3), 409–424.
Weinstein, Y.S., 1998. Mechanisms of generation of intra-continental alkali-basalts in northeastern Israel. Ph.D. Thesis, Hebrew Univ., Jerusalem, 101 p.
Woodside, J.M., 1977. Tectonic elements and crust of the eastern Mediterranean Sea. Mar. Geophys. Res. 3, 317–354.
Worrall, D.M., Snelson, S., 1989. Evolution of the northern Gulf of Mexico, with emphasis on Cenozoic growth faulting and the role of salt. In: Bally, A.W., Palmer, A.R. (Eds.), The Geology of North America: an Overview. Geol. Soc. Am., A, pp. 97–138.
Zak, I., 1967. The geology of Mount Sedom. Ph.D. Thesis, Hebrew Univ., Jerusalem (in Hebrew, English summary), 208 p.
Zilberman, E., 1992. Remnants of Miocene landscape in the central and northern Negev and their paleogeographic implications. Isr. Geol. Surv. Bull. 83. 54 pp.